

Tracing Multilingual Representations in LLMs with Cross-Layer Transcoders

Abir Harrasse ^{*1 2 3} Florent Draye ^{*1} Punya Syon Pandey ^{4 5} Zhijing Jin ^{1 4 5} Bernhard Schölkopf ^{1 6}

Abstract

Multilingual Large Language Models (LLMs) can process many languages, yet how they internally represent this diversity remains unclear. Do they form shared multilingual representations with language-specific decoding, and if so, why does performance favor the dominant training language? To address this, we train models on different multilingual mixtures and analyze their internal mechanisms using *Cross-Layer Transcoders* (CLT) and *Attribution Graphs*. Our results reveal multilingual shared representations: the model employs highly similar features across languages, while language-specific decoding emerges in later layers.

Training models without English shows identical multilingual shared space structures. Decoding relies partly on a small set of high-frequency features in the final layers, which linearly encode language identity from early layers. Intervening on these features allows one language to be suppressed and another substituted. Finally, to explain non-English failures, we perform a *Model-Diffing* experiment: underperformance arises from dim late-layer features, weak middle-layer clusters, and tokenizer bias toward English that forces early layers to specialize in word reassembly. Finetuning strengthens these features and their links, improving token assembly and language-specific decoding, providing a mechanistic explanation for multilingual gaps.

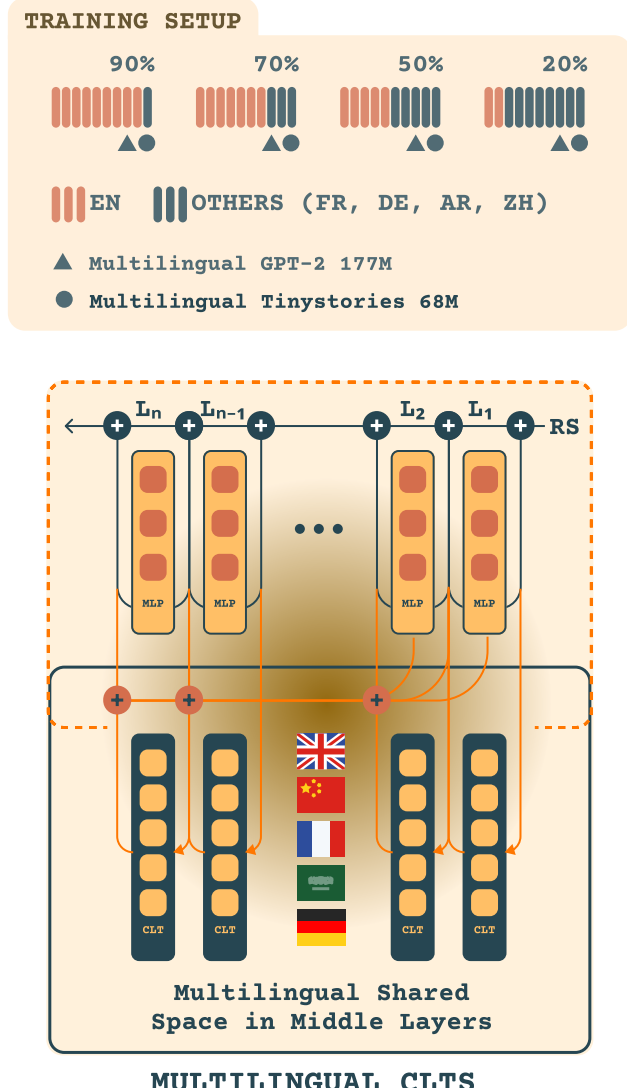


Figure 1. Cross-Layer Transcoders (CLTs) (Ameisen et al., 2025) (bottom) reveal that multilingual LLMs (middle) consistently form a shared language-agnostic space in middle layers (gradient middle region) where all languages converge, regardless of English dominance in the training mixtures (top).

1. Introduction

The inclusion of diverse languages in the large-scale training data of LLMs (Grattafiori et al., 2024; Team et al., 2024;

¹Max Planck Institute for Intelligent Systems, Tübingen, Germany ²Mohammed VI Polytechnic University, Morocco ³Martian ⁴University of Toronto, Canada ⁵Vector Institute, Canada ⁶ELLIS Institute, Tübingen, Germany. Correspondence to: Abir Harrasse <aharrasse@cs.toronto.edu>, Florent Draye <florent.draye@tuebingen.mpg.de>, Zhijing Jin <zjin@cs.toronto.edu>.

Brown et al., 2020; Chowdhery et al., 2022) has led to remarkable multilingual capabilities (Shi et al., 2022; Conneau et al., 2020a; Workshop et al., 2023). However, the underlying mechanisms driving their multilingual behavior remain poorly understood. For example, do LLMs form shared multilingual representations in their internal layers, so, why does performance still favor the dominant training language, such as English? Prior mechanistic investigations have yielded *conflicting findings* about multilingual processing. While some work maps inputs into English-aligned latent spaces and suggests that LLMs process non-English inputs through English-biased representations (Wendler et al., 2024; Schut et al., 2025), other studies find evidence of shared cross-lingual grammatical structures encoded in common feature directions (Brinkmann et al., 2025). Moreover, all existing approaches rely primarily on *static* probing methods that cannot capture the *dynamic transformation* of linguistic information across model layers.

To address the aforementioned limitations, we derive attribution graphs from our self-trained cross-layer transcoders (Ameisen et al., 2025), a recent advance in mechanistic interpretability, which can track feature interactions across layers and provide the first mechanistic account of how LLMs transition between shared and language-specific processing modes. Our results suggest that all languages have a shared representation in LLMs’ internal layers, which we call as a “pivot language.” We also discover language-specific decoding in later layers to handle their multilingual output generation.

Depending on our CLT-driven insights, we conduct two causal studies. First, we are able to change the output language by intervening on a small set of high-frequency language features in the final layers decoding from the pivot language to the target language. Further, we investigate the causal effect of training data composition by varying English-to-multilingual ratios. We analyze our re-trained models on different language ratios, and reveal how language distribution during pretraining shapes internal multilingual representations. Our contributions are as follows:

1. We find that multilingual LLMs form shared multilingual representations, relying on consistent internal circuits to process equivalent queries across languages. These structures emerge even without English or a dominant language, indicating that pivot mechanisms are an architectural property rather than a consequence of language dominance. While English-dominant models may still preferentially align with English, it is not strictly required for the emergence of shared representations.
2. We show that language decoding primarily depends on a small set of high-frequency language features in the

late layers that read off information from early layer features and tokens embeddings.

3. We identify and characterize language-specific failure modes, where models succeed in English but fail on equivalent inputs in other languages, linking these disparities to underlying mechanisms.
4. We release nine multilingual models¹ (two sizes \times four data mixtures + non-English model), three finetuned models and their corresponding cross-layer transcoders (CLTs)², trained on balanced language distributions to support cross-lingual analysis and transfer. We also release our codebase³.

2. Related Work

2.1. Multilingual Language Models

Multilingual language models have evolved from early architectures like mBERT (Devlin et al., 2019) to sophisticated models such as XLM-R (Conneau et al., 2020b), LLaMA (Touvron et al., 2023), and Gemma (Team et al., 2024). Despite their impressive capabilities, systematic performance disparities persist across languages (Pires et al., 2019; Hu et al., 2020). English consistently outperforms other languages, particularly for low-resource languages and complex reasoning tasks (Lauscher et al., 2020; Shi et al., 2022). Benchmarks like XTREME (Hu et al., 2020) and XNLI (Conneau et al., 2020b) have documented these gaps across language families. The English-dominant training data composition has been hypothesized as a primary factor (Bender et al., 2021), though the underlying mechanisms driving these disparities remain poorly understood.

2.2. Internal Representations and the Pivot Hypothesis

Recent investigations have revealed that multilingual LLMs process non-English inputs through English-aligned latent representations. Wendler et al. (2024) used logit lens analysis to show that intermediate layers predict English tokens before target-language tokens. Similarly, Schut et al. (2025) demonstrated systematic bias toward English-like representations regardless of input language. These findings suggest models internally translate to English, perform reasoning, then translate back, a mechanism that has been leveraged through embedding alignment (Lample & Conneau, 2019; Artetxe et al., 2018), translation-based fine-tuning (Zhu et al., 2024), and romanization strategies for non-Latin scripts (Saji et al., 2025).

Prompting strategies also exploit this English-pivot behav-

¹Models: Multilingual TinyStories and Multilingual GPT-2

²CLTs: Multilingual CLTs

³Code: <https://github.com/abirharrasse/MultilingualCLTs>

ior, including direct prompt translation (Shi et al., 2022; Ahuja et al., 2023; Etxaniz et al., 2023) and English chain-of-thought reasoning (Wei et al., 2022; Vatsal et al., 2025). While some grammatical features exhibit universal representations across languages (Brinkmann et al., 2025), lexical and semantic processing appears more language-specific (Chi et al., 2020).

These observations align with the recently proposed “Platonic hypothesis” (Huh et al., 2024), which suggests that models converge toward abstract, unified representations capturing conceptual essences beyond surface forms. The shared multilingual space behavior, where models develop language-agnostic representations before language-specific decoding, provides some empirical support for this hypothesis in multilingual settings.

2.3. Mechanistic Interpretability in LLMs

Mechanistic interpretability seeks to understand transformer internals through circuit analysis (Olah et al., 2020; Elhage et al., 2021). Early work identified specific circuits for behaviors like indirect object identification (Wang et al., 2022) and induction heads (Olsson et al., 2022). Sparse Autoencoders (SAEs) decompose representations into interpretable features (Cunningham et al., 2023; Templeton et al., 2024), while transcoders directly model MLP outputs rather than autoencoding activations (Dunefsky et al., 2024).

Cross-Layer Transcoders (CLTs) advance this approach by assigning distinct decoder matrices per downstream layer, significantly simplifying feature graphs and enabling tractable circuit analysis (Ameisen et al., 2025; Hanna et al., 2025). However, CLT applications remain limited—primarily Anthropic’s foundational work (Lindsey et al., 2025b), a “greater-than” mechanism study (Merullo et al., 2025), and recent open-source extensions (Lindsey et al., 2025a). This scarcity reflects the considerable challenges in training CLTs at scale.

For multilingual models, mechanistic analyses are particularly sparse. Beyond Wendler et al. (2024)’s logit lens study and Anthropic’s case study (Lindsey et al., 2025b), our work represents the first comprehensive CLT-based investigation of multilingual processing. Crucially, ensuring fair cross-language comparisons requires training CLTs on balanced multilingual distributions to avoid feature bias toward dominant languages.

3. Experimental Setup and Methods

3.1. Mixture of multilingual LLMs

We study the multilingual behavior of LLMs across five languages: English, German, French, Arabic, and Chinese. To investigate how training data composition affects inter-

nal representations, we train four GPT-2 style models (12 layers, ~ 177.6 M parameters) on a realistic web mixture (OpenWebText + FineWeb2 (Penedo et al., 2025)), and four tiny-stories style models (4 layers and ~ 68.5 M parameters) on a controlled narrative dataset (TinyStories translated into all five languages). Finally, we include an *off-the-shelf* LLaMA-3.2-1B model (Meta AI, 2026) for comparison.

To facilitate our training data manipulation study, we investigate training data settings where all languages are evenly distributed vs those with one dominant language. To investigate the effect of a dominant language, we vary the English proportion in the data from dominant (90%) to balanced (20%), with the remaining data evenly split across the other four languages. All models use debiased tokenizers trained on evenly distributed five-language data, so that differences in internal representations reflect the training distribution rather than tokenization artifacts. Figure 1 illustrates the training configurations.

3.2. Cross-Layer Transcoders (CLTs)

To probe internal multilingual mechanisms, we employ CLTs, which map activations between layers to reveal how semantic representations evolve during processing. A CLT consists of neurons (features) divided into encoder and decoder components.

Formally, to run a cross-layer transcoder, let $\mathbf{h}_\ell \in \mathbb{R}^{d_{\text{model}}}$ be the input to the MLP at layer ℓ for single token position. We define

$$\mathbf{z}_\ell = \text{ReLU}(\mathbf{W}_{\text{enc}}^\ell \mathbf{h}_\ell + \mathbf{b}_{\text{enc}}^\ell) \in \mathbb{R}^{d_{\text{features}}}, \quad (1)$$

where $\mathbf{W}_{\text{enc}}^\ell \in \mathbb{R}^{d_{\text{features}} \times d_{\text{model}}}$ is the encoder weight matrix and $\mathbf{b}_{\text{enc}}^\ell \in \mathbb{R}^{d_{\text{features}}}$ is the encoder bias. The CLTs then reconstructs the MLP output at layer ℓ' as

$$\hat{\mathbf{m}}_{\ell'} = \sum_{\ell \leq \ell'} \mathbf{W}_{\text{dec}}^{\ell \rightarrow \ell'} \mathbf{z}_\ell + \mathbf{b}_{\text{dec}}^{\ell'}, \quad (2)$$

where $\mathbf{W}_{\text{dec}}^{\ell \rightarrow \ell'} \in \mathbb{R}^{d_{\text{model}} \times d_{\text{features}}}$ is the decoder matrix from layer ℓ to ℓ' .

Following Anthropic guidelines (Ameisen et al., 2025), the final training objective is

$$\begin{aligned} \mathcal{L} = & \underbrace{\sum_{\ell'} \|\hat{\mathbf{m}}_{\ell'} - \mathbf{m}_{\ell'}\|_2^2}_{\text{MSE reconstruction}} \\ & + \lambda_0 \underbrace{\sum_{\ell} \tanh(C(\mathbf{z}_\ell \odot \|\mathbf{W}_{\text{dec}}^\ell\|))}_{L_0 \text{ sparsity}} \\ & + \lambda_{\text{df}} \underbrace{\sum_{\ell} \text{ReLU}(\exp(\tau) - \mathbf{h}_\ell^{\text{pre}}) \|\mathbf{W}_{\text{dec}}^\ell\|}_{\text{dead feature penalty}}, \end{aligned} \quad (3)$$

where $\mathbf{W}_{\text{dec}}^\ell$ are concatenated decoder weights for layer ℓ , $\mathbf{h}_\ell^{\text{pre}}$ are pre-activation values, τ is a threshold parameter, and C is a scaling constant. λ_0 and λ_{df} control the strength of the sparsity and dead-feature regularization terms.

We train CLTs on activation vectors sampled uniformly across languages until convergence. Training details, hyper-parameters, and performance metrics appear in Appendix B.

3.3. Graph attribution

Following Ameisen et al. (2025), we compute the attribution score between every feature n at layer ℓ , position k , and feature n' at layer ℓ' , position k' , as

$$a_{\ell,k,n}^{\ell',k',n'} = \sum_{\ell \leq s \leq \ell'} f_{k,n}^{\ell \rightarrow s} J_{s,k}^{\ell',k'} g_{k',n'}^{\ell'}, \quad (4)$$

where $f_{k,n}^{\ell \rightarrow s}$ denotes the vector for feature n in the decoder matrix projecting from layer ℓ to s , $J_{s,k}^{\ell',k'}$ is the Jacobian between the MLP output at (ℓ, k) and the MLP input at (ℓ', k') , computed during a forward pass where nonlinearities (normalization layers, attention computations, and MLPs) are frozen using stop-gradient operations, and $g_{k',n'}^{\ell'}$ is the corresponding encoder feature at layer ℓ' and position k' . The graph is then pruned to retain only features that cumulatively account for 80% of the effect on the final logit, and edges that cumulatively account for 95% of the edge effect on the final logit. We use the circuit-tracer library (Hanna et al., 2025).

3.4. Multilingual Score

For each CLT feature f , we compute the multilingual scores on both the top 100 most activated sequences for that feature and on a general sample of 600k sequences balanced across the five languages (each of length 16). If a feature is active for at least one token in a sequence, it is considered active for that sequence. Since each sequence corresponds to a specific language, this allows us to compute a normalized activation distribution:

$$p_l(f) = \frac{A_l(f)}{\sum_{l'} A_{l'}(f)}, \quad (5)$$

where $A_l(f)$ is the number of sequences in language l for which feature f is active. We then define the multilingual score for feature f as the entropy of this distribution:

$$H(f) = - \sum_{l=1}^L p_l(f) \log p_l(f), \quad L = 5, \quad (6)$$

which measures multilinguality: low $H(f)$ indicates language-specific features, while high $H(f)$ indicates multilingual features. We normalize the entropy scores to have scores between 0 and 1.

4. Results

We organize our results around three core questions that progressively unpack how multilingual representations emerge and operate in large language models:

1. Do models form shared multilingual representations or a pivot language across data mixtures? (Section 4.1)
2. How do models decode language identity and route information to the correct output language? (Section 4.2)
3. Why do models still fail in non-English settings despite shared representations? (Section 4.3)

4.1. Emergence of a Pivot Language

4.1.1. GENERALIZATION UNDER DATA IMBALANCE

We begin by assessing whether models trained on imbalanced multilingual mixtures are still able to generalize across languages. Figure 11 reports the validation cross-entropy losses for models trained with varying proportions of English tokens, including extreme settings where English accounts for 90% of the training data. Despite this imbalance, the models achieve competitive validation performance not only in English but also in minority languages such as Arabic, indicating that the learned representations capture transferable features rather than being restricted to high-resource languages. Together, these results suggest that multilingual circuits remain robust under imbalance and motivate a deeper investigation into how such robustness is organized within the model. More results are presented in Appendix C.

4.1.2. LANGUAGE ENTROPY ACROSS LAYERS

To investigate how multilingual representations are distributed within the network, we analyze the language entropy of feature activations at each layer. For each feature, we compute the multilingual score $H(f)$ as defined in Section 3.4, and multiply it by its corresponding activation rate computed over a large subset of the training data (4M Tokens). Figure 2 shows the resulting average weighted entropy for the top100 score across layers for models trained on different data mixtures.

Here we summarize three major findings on the layerwise organization of multilingual representations:

Finding 1. Layerwise entropy follows a U-shaped trend. Entropy is relatively low in early layers, rises sharply in the middle layers, and decreases again toward the output layers. This indicates that early layers primarily encode language-specific features, middle layers integrate information into

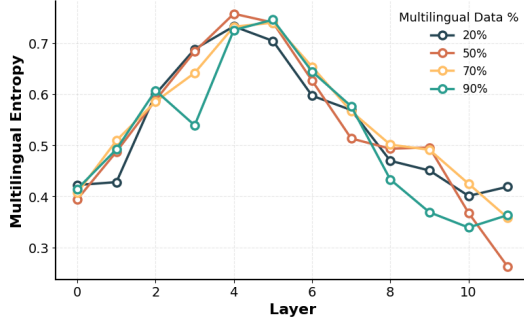


Figure 2. Rate-weighted multilingual score $H(f)$ across layers, showing that middle layers consistently form a multilingual space, while early and late layers are more language-specific. This pattern holds across model sizes and training data mixtures.

a shared multilingual space, and later layers partially re-specialize for language-specific decoding.

Finding 2. The trend is robust across data mixtures and model scales. The emergence of a shared multilingual latent space in the middle layers is stable across different training data, and we also observe this well-defined behavior in the Llama-3.2-1B CLTs (see Figure 20), showing generalization to larger models.

Finding 3. Model depth influences the behavior. For the 4-layer TinyStories model, the up-and-down pattern is absent and all layers have similar entropy scores (Figure 20), suggesting a minimum model size for this behavior to emerge.

The behavior is similar for the general entropy score. A discussion comparing the top100 score and the overall training distribution score is provided in Appendix E. These findings complement the validation loss results and provide quantitative evidence that the model organizes its internal representations to support cross-lingual generalization.

Shared Multilingual Space Independence from English. To validate that shared multilingual space structures do not require English dominance, we trained GPT-2 on balanced non-English data (25% French, 25% German, 25% Arabic, 25% Chinese) and computed weighted multilingual entropy across layers. The resulting curve exhibits the identical characteristic rise-and-fall pattern observed in English-dominant models, with peak entropy in layers 5-6 (Figure 22). This demonstrates that the shared multilingual space emergence is a fundamental architectural property, not an artifact of English dominance.

4.1.3. MULTILINGUAL CIRCUITS ACROSS DATA MIXTURES

To complement the multilingual score analysis, we extract attribution graphs to identify circuits active across data mix-

tures. We focus on two sentence types: (i) preposition sentences, where the model predicts a function word such as in J’ai bu une tasse or It was a piece, and (ii) content word sentences, where it predicts a meaningful token such as I prefer drinking tea to drinking in the 90% English mixture or Winter, spring, summer, and autumn are the four in the 20% mixture. We also analyze examples involving calendar terms (Monday, Tuesday, Wednesday, Thursday) and analogy prompts (the opposite of ‘men’ is...). Figure 3 shows two representative circuits, one for an English preposition and one for a German content word, with remaining examples in Appendix G.1 and more details about the clustering and cluster’s entropy calculation in Appendix G.

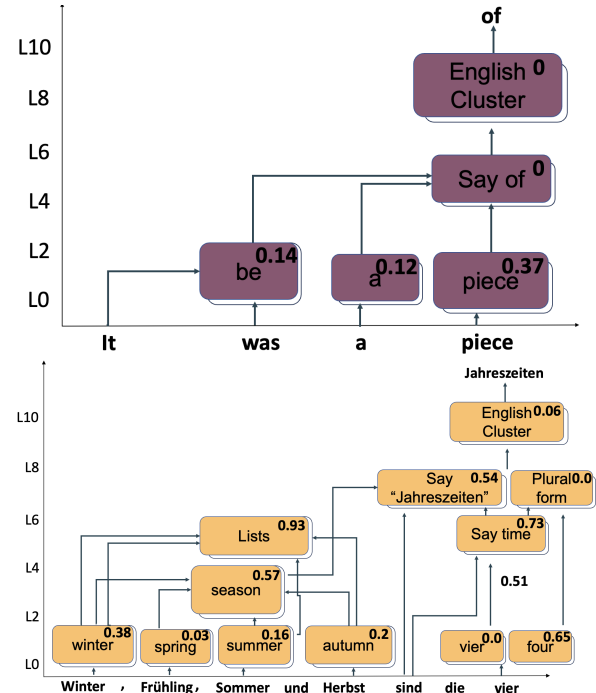


Figure 3. Circuits identified across different training data mixtures. Middle layers consistently form multilingual clusters, while early and late layers remain more language-specific. The scores at the top right of each cluster indicate language entropy (higher values correspond to more multilingual clusters). The patterns are stable across mixtures, sentence types, and languages.

Here we summarize three main findings on multilingual circuits across layers and data mixtures:

Finding 1. Layerwise organization exhibits a three-phase structure: early and late layers are mostly language-specific, while middle layers form dense multilingual clusters. Circuits for determiners remain largely language-specific, confirming observations from Schut et al. (2025).

Finding 2. Semantic alignment can emerge early or late depending on the data. In some cases in the 90% English model, the late-layer English cluster is missing, suggesting

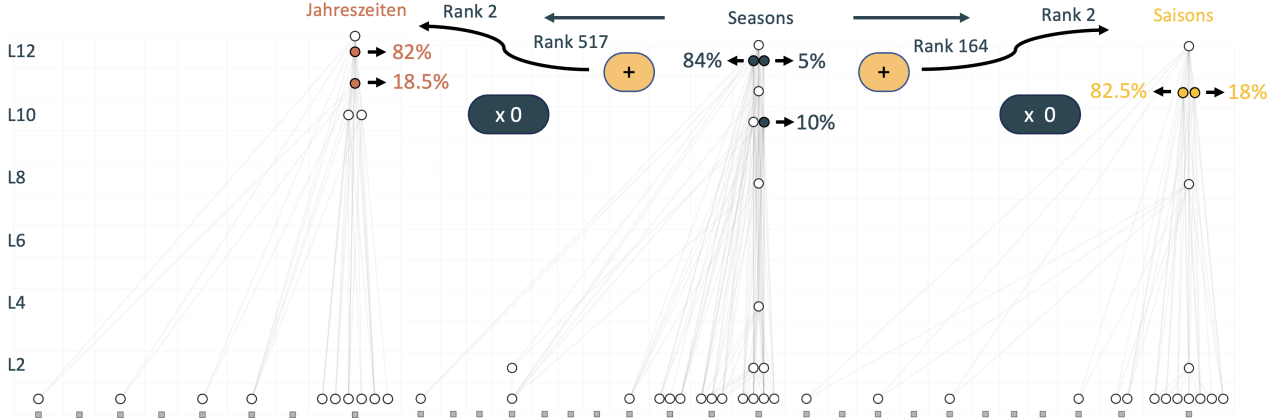


Figure 4. Attribution graphs in French, English, and German for the 20% model pruned at 50% for the prompt “Autumn, Winter, Fall, and Spring are the four”. Interventions are displayed and language features highlighted in color with their corresponding percentage of activation on their language.

the model does not always rely on English for semantic grounding. Conversely, layer 0 sometimes already shows multilingual alignment. When tokenization is clean, the first attention and MLP blocks link semantically equivalent tokens across languages, indicating that semantic mapping begins from the very first layer. In the 20% mixture, Arabic features link words sharing historical meanings, such as connecting “qalb” (“heart”) to its older sense of “change” or “transformation,” showing that the model recovers deep etymological relations.

Finding 3. Performance and representation quality are affected by tokenization. The model’s weaker performance on Arabic partially results from tokenization. Even with a balanced multilingual tokenizer, Arabic words are frequently split into small fragments, forcing the first layers (up to layer 3) to focus on reassembling words rather than learning higher-level meaning (Figures 25b and 26b).

4.2. Mechanisms of Language Decoding

A central question in multilingual models with pivot languages is how models encode language information and integrate it in final layers to predict the correct next token. Across all graphs, language-specific features appear predominantly in early and late layers. In early layers, these features often correspond to single-token content rather than language alone. As in (Lindsey et al., 2025b), we find early-layer features indicating output language for specific contexts (e.g., after quotation marks in “The opposite of “men” is “”), but these features are not consistently present in general cases.

Finding 1. Across all attribution graphs, we find that late-layer language clusters drive decoding. These clusters correspond to high-frequency features that activate for large

proportions of tokens within their respective languages. As shown in Appendix D, Figure 18, most high-frequency CLT features are language-specific. Figure 4 shows that these late-layer activations can be linearly read from early-layer features and embedding nodes, indicating that language identity propagates hierarchically through the model.

Finding 2. Direct intervention experiments confirm the causal role of these clusters in controlling output language. Zeroing late-layer language features for one language and adding those from a target language (using activations from translated prompts) substantially increases the target-language logit rank. Perfect prediction typically requires additional feature modifications or sweeping intervention values.

Finding 3. Finally, activation frequency patterns reveal both language ambiguity and dominance effects. As shown in Figure 5, a small number of features activate on 50–100% of tokens within each language, while inactive tokens occur mostly at sequence beginnings where language identity is ambiguous (especially between French, English, and German). Dominant languages exhibit fewer high-frequency features than others across both GPT-2 and LLaMA models, suggesting that English functions as a default output language requiring fewer explicit high-frequency features (Lindsey et al., 2025b).

Language-specific features exhibit significant overlap with English features that increases with English training proportion (77% to 84%), while non-English languages maintain stronger mutual feature overlap (89%) that progressively converges toward English at higher proportions. This pattern indicates that the shared multilingual space emergence is partly driven by training data composition, with English acting as a convergence point (Appendix D).

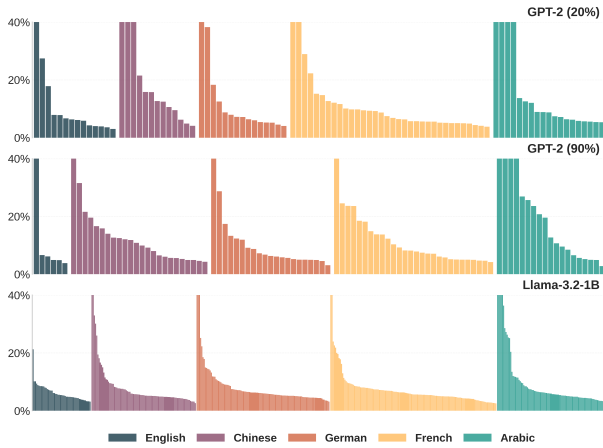


Figure 5. Frequency of token activations over their respective languages of the language features for the 20% model.

4.3. Failure Mechanisms in Non-English Languages

As shown in Section 4.1.3, multilingual LLMs develop shared representations in their middle layers, indicating that equivalent meanings are processed via common internal mechanisms across languages. Despite this, models consistently perform better on English, and even models trained on uniformly distributed multilingual data show a persistent English bias. This raises a key question: if the model relies on shared circuits, why does this performance gap persist?

To address this, we analyze failure and repair mechanisms in non-English languages using a **model-diffing approach**. Intuitively, the features a model adjusts to perform better in a language reveal what it struggles with most. Let \mathcal{M}_0 denote the base multilingual model, and \mathcal{M}_ℓ a version finetuned on language ℓ . We finetune the original CLT (trained on activations from \mathcal{M}_0) on the activations of \mathcal{M}_ℓ to identify the features the model modifies to improve performance. We denote the corresponding feature dictionaries as \mathcal{D}_0 and \mathcal{D}_ℓ .

We present the findings from our model-diffing experiments on low-performing languages $\ell \in \{\text{Arabic, Chinese, German}\}$. Our goal is to understand which features and layers \mathcal{M}_ℓ adjusts relative to the base model \mathcal{M}_0 , and how these changes propagate to token-level representations.

4.3.1. MODELS REPAIR IN LATER LAYERS

For each language ℓ , we compute the cosine similarity between the feature dictionaries \mathcal{D}_0 and \mathcal{D}_ℓ across layers.

Figure 6 shows that the largest changes occur in the later layers. This finding aligns with our previous observation that language-specific features are predominantly located in

these layers. It is intuitive that the model focuses on refining these representations: by strengthening their connection to the multilingual shared space in the middle layers, \mathcal{M}_ℓ can more effectively translate and map language-specific inputs to shared high-level representations, ultimately improving performance.

4.3.2. REPAIR THROUGH MULTILINGUAL FEATURE CHANGES

To understand how finetuning affects multilingual representations, we split features in each layer into two buckets based on cosine similarity: high-change features ($\text{cos-sim}(\mathcal{D}_0, \mathcal{D}_\ell) < 0.5$) and low-change features ($\text{cos-sim}(\mathcal{D}_0, \mathcal{D}_\ell) \geq 0.5$).

Figure 7 shows the distribution of high-change features across layers. Across all languages, high-change features are concentrated in late layers, consistent with our previous analysis. Interestingly, we observe additional patterns in the early and late layers:

- **Layer 0 (embedding layer):** Features remain largely unchanged, indicating that the model preserves the base token embeddings.
- **Layer 1:** Changes primarily eliminate reductions for Chinese, while English and French dominate the remaining high-change features. This suggests early-layer adjustments help align language-specific signals with shared representations.
- **Layer 11 (late layer):** Most transformative changes occur here. High-change features (*bucket 1*) consistently increase probabilities for the target language across all languages, indicating that the model performs subtle adjustments—minor rotations or rescaling—to align language-specific features with the correct output while maintaining stable, well-behaved representations.

These adjustments naturally push features from other languages into *bucket 2* (low similarity), balancing the representation space. Notably, we also observe cross-language effects: finetuning German increases Arabic features in *bucket 1*, and Chinese exhibits similar interactions with French and Arabic. This hints at overlapping subspaces between languages, where modifications in one language can partially transfer to others. More results and experimental setup are shown in Appendix J.1.

4.3.3. CAUSAL IMPACT OF HIGH-CHANGE FEATURES

To assess the functional role of the high-change features identified in \mathcal{D}_ℓ , we perform a causal analysis using LogitLens. For a given high-change feature $f \in \mathcal{D}_\ell$ and \mathcal{D}_0 , we compute its top aligned tokens via the unembedding matrix:

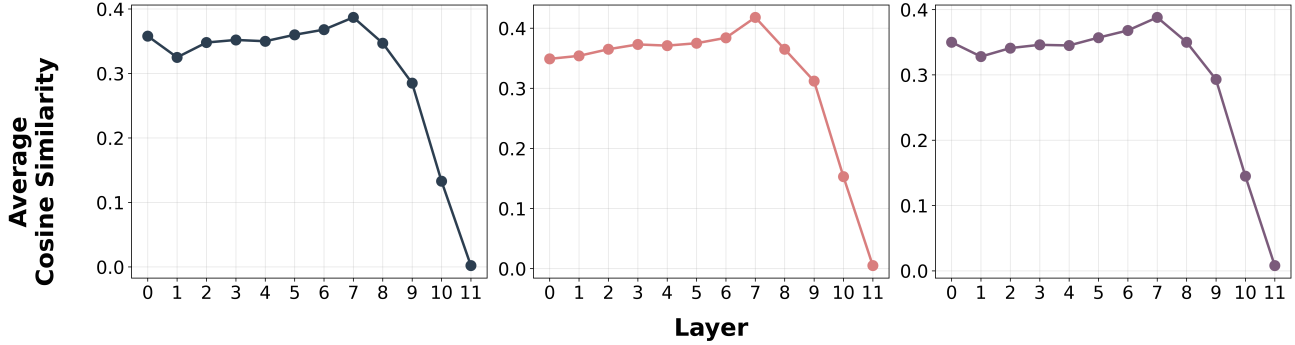


Figure 6. Cosine similarity between \mathcal{D}_0 and \mathcal{D}_ℓ across layers for Arabic (left), German (middle) and Chinese (right). The largest representation changes occur in the late layers, indicating that the model focuses its most transformative adaptations there.

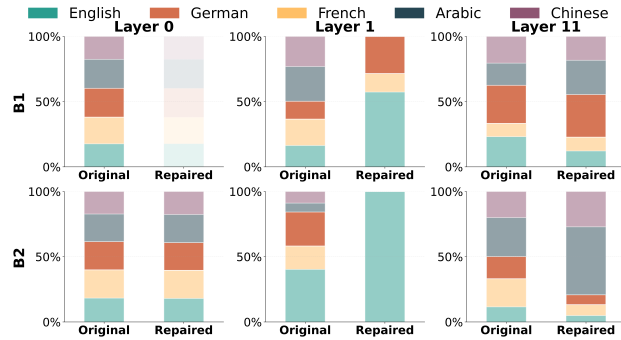


Figure 7. Language distribution comparison across layers for German. Middle layers show high entropy and low language distribution deltas and are therefore omitted from the figure. Results for Arabic and Chinese are presented in Appendix J.1

$$\mathbf{t}^*(\mathbf{f}) = \arg \max_i [W_U W_{\text{dec}} f]_i,$$

where W_{dec} is the decoder projection and W_U is the unembedding matrix. This operation identifies the tokens most strongly influenced by \mathbf{f} .

We find that, after finetuning, these features contribute to increased token assembly in early layers (see Figure 43). This suggests that late-layer adaptations in \mathcal{D}_ℓ propagate backward, enabling \mathcal{M}_ℓ to construct more abstract, compositional representations. Furthermore, the norms of high-change features in \mathcal{D}_ℓ are larger than in \mathcal{D}_0 , reflecting stronger and more confident activations.

For further details on the features analyzed and the results of the Logit Lens experiment, see Appendix J.2.

4.3.4. CIRCUIT-LEVEL ILLUSTRATION

To illustrate our findings, we present over 40 representative circuit examples from Arabic, Chinese, and German (full details in Appendix G.2). These examples show how interventions that activate clusters of high-change features

can improve the model’s retrieval of the correct answer. We further observe that sub-tokenization weakens edges to the most important clusters, and that the tokenizer—despite being trained on equal amounts of data per language—exhibits a bias toward English. This bias provides a mechanistic explanation for the performance gaps observed across languages.

5. Conclusion

We present a mechanistic account of multilingual processing in LLMs using Cross-Layer Transcoders, showing that models form shared multilingual representations in their middle layers while relying on small sets of high-frequency features for language-specific decoding. These features linearly read out language identity from earlier layers, and targeted interventions on them can reliably shift the model’s output language. Performance differences across languages seem to arise less from missing multilingual circuits and more from factors such as tokenization and the strength of downstream activations. Overall, our results show how CLTs make it possible to pinpoint where multilingual disparities emerge and provide a practical basis for more focused investigations of cross-language processing in LLMs.

Limitations

Model Scale and Architecture. Our primary analysis focuses on relatively small models (68M and 177M parameters) trained from scratch. While we include LLaMA-3.2-1B for validation and observe consistent patterns, our findings may not fully generalize to production-scale models (10B+ parameters) or models trained with different architectural choices. Larger models may develop additional mechanisms or more nuanced multilingual representations that our current analysis does not capture.

Tokenization Analysis. While we identify tokenization as a critical factor in performance disparities, our analy-

sis uses a single BPE-based tokenizer trained on balanced data. We do not systematically compare alternative tokenization strategies (e.g., character-level, morpheme-aware, or language-specific tokenizers) that might better preserve semantic information across scripts. The optimal tokenization approach for multilingual models remains an open question.

Reproducibility Constraints. The computational cost of training both base models and CLTs (requiring thousands of GPU-hours) may limit independent replication. While we release our models and CLTs, the specific training dynamics and their sensitivity to random seeds, hardware variations, and implementation details have not been exhaustively characterized.

Impact Statement

CLTs make it possible to trace multilingual processing step by step—from early encoding through shared representations to language-specific decoding—revealing where mechanisms are shared across languages and where they diverge. This enables a concrete, mechanistic view of language disparities: rather than relying solely on task-level performance, we can directly identify circuits that are weaker, missing, or more fragmented for particular languages. Using this lens, we show that even under balanced training data, multilingual models exhibit systematic gaps; for example, Arabic is heavily sub-tokenized, requiring early layers to reconstruct fragmented words. We release our models and CLTs to support further research, while noting that training required thousands of GPU-hours and that intervention capabilities raise fairness and misuse considerations. Although our experiments focus on five languages and relatively small models, the approach provides a structured foundation for analyzing multilingual processing and developing more equitable multilingual AI systems.

Acknowledgment

We thank Michael Hanna for insightful discussions on the added value of Cross-Layer Transcoders compared to Single-Layer Transcoders, as well as on the training challenges and implementation details of CLTs. We are grateful to Anson Lei for his assistance with the trained GPT-2 model generation issue and for sharing tips on prompt formatting. We also thank Francesco Ortu for his valuable feedback, which helped improve the clarity and flow of the paper and Antia Garcia for helping improve the design of the main figure.

This material is based in part upon work supported by the German Federal Ministry of Education and Research (BMBF): Tübingen AI Center, FKZ: 01IS18039B; by the Machine Learning Cluster of Excellence, EXC number 2064/1 – Project number 390727645; by Schmidt Sciences

SAFE-AI Grant; by the Frontier Model Forum and AI Safety Fund; by Open Philanthropy; by the Cooperative AI Foundation; and by the Survival and Flourishing Fund. Resources used in preparing this research were provided, in part, by the Province of Ontario, the Government of Canada through CIFAR, and companies sponsoring the Vector Institute. F.D. acknowledges support through a fellowship from the Hector Fellow Academy. We gratefully acknowledge EleutherAI for providing compute resources that enabled the Cross-Layer Transcoder finetuning in our model-diffing experiments.

References

Ahuja, K., Diddee, H., Hada, R., Ochieng, M., Ramesh, K., Jain, P., Nambi, A., Ganu, T., Segal, S., Axmed, M., Bali, K., and Sitaram, S. *Mega: Multilingual evaluation of generative ai*, 2023. URL <https://arxiv.org/abs/2303.12528>.

Ameisen, E., Lindsey, J., Pearce, A., Gurnee, W., Turner, N. L., Chen, B., Citro, C., Abrahams, D., Carter, S., Hosmer, B., Marcus, J., Sklar, M., Templeton, A., Bricken, T., McDougall, C., Cunningham, H., Henighan, T., Jermyn, A., Jones, A., Persic, A., Qi, Z., Ben Thompson, T., Zimmerman, S., Rivoire, K., Conerly, T., Olah, C., and Batson, J. *Circuit tracing: Revealing computational graphs in language models*. *Transformer Circuits Thread*, 2025. URL <https://transformer-circuits.pub/2025/attribution-graphs/methods.html>.

Artetxe, M., Labaka, G., and Agirre, E. Generalizing and improving bilingual word embedding mappings with a multi-step framework of linear transformations. *Proceedings of the AAAI Conference on Artificial Intelligence*, 32(1), Apr. 2018. doi: 10.1609/aaai.v32i1.11992. URL <https://ojs.aaai.org/index.php/AAAI/article/view/11992>.

Bender, E. M., Gebru, T., McMillan-Major, A., and Shmitchell, S. On the dangers of stochastic parrots: Can language models be too big? In *Proceedings of the 2021 ACM Conference on Fairness, Accountability, and Transparency*, FAccT ’21, pp. 610–623, New York, NY, USA, 2021. Association for Computing Machinery. ISBN 9781450383097. doi: 10.1145/3442188.3445922. URL <https://doi.org/10.1145/3442188.3445922>.

Brinkmann, J., Wendler, C., Bartelt, C., and Mueller, A. Large language models share representations of latent grammatical concepts across typologically diverse languages, 2025. URL <https://arxiv.org/abs/2501.06346>.

Brown, T. B., Mann, B., Ryder, N., Subbiah, M., Kaplan, J., Dhariwal, P., Neelakantan, A., Shyam, P., Sastry, G.,

Askell, A., Agarwal, S., Herbert-Voss, A., Krueger, G., Henighan, T., Child, R., Ramesh, A., Ziegler, D. M., Wu, J., Winter, C., Hesse, C., Chen, M., Sigler, E., Litwin, M., Gray, S., Chess, B., Clark, J., Berner, C., McCandlish, S., Radford, A., Sutskever, I., and Amodei, D. Language models are few-shot learners, 2020. URL <https://arxiv.org/abs/2005.14165>.

Chi, E., Hewitt, J., and Manning, C. D. Finding universal grammatical relations in multilingual bert. In *ACL*, 2020.

Chowdhery, A., Narang, S., Devlin, J., Bosma, M., Mishra, G., Roberts, A., Barham, P., Chung, H. W., Sutton, C., Gehrmann, S., Schuh, P., Shi, K., Tsvyashchenko, S., Maynez, J., Rao, A., Barnes, P., Tay, Y., Shazeer, N., Prabhakaran, V., Reif, E., Du, N., Hutchinson, B., Pope, R., Bradbury, J., Austin, J., Isard, M., Gur-Ari, G., Yin, P., Duke, T., Levskaya, A., Ghemawat, S., Dev, S., Michalewski, H., Garcia, X., Misra, V., Robinson, K., Fedus, L., Zhou, D., Ippolito, D., Luan, D., Lim, H., Zoph, B., Spiridonov, A., Sepassi, R., Dohan, D., Agrawal, S., Omernick, M., Dai, A. M., Pillai, T. S., Pellan, M., Lewkowycz, A., Moreira, E., Child, R., Polozov, O., Lee, K., Zhou, Z., Wang, X., Saeta, B., Diaz, M., Firat, O., Catasta, M., Wei, J., Meier-Hellstern, K., Eck, D., Dean, J., Petrov, S., and Fiedel, N. Palm: Scaling language modeling with pathways, 2022. URL <https://arxiv.org/abs/2204.02311>.

Conneau, A., Khandelwal, K., Goyal, N., Chaudhary, V., Wenzek, G., Guzmán, F., Grave, E., Ott, M., Zettlemoyer, L., and Stoyanov, V. Unsupervised cross-lingual representation learning at scale. In *Proceedings of ACL 2020*, 2020a. URL <https://aclanthology.org/2020.acl-main.747>.

Conneau, A., Khandelwal, K., Goyal, N., Chaudhary, V., Wenzek, G., Guzmán, F., Grave, E., Ott, M., Zettlemoyer, L., and Stoyanov, V. Unsupervised cross-lingual representation learning at scale, 2020b. URL <https://arxiv.org/abs/1911.02116>.

Cunningham, E. et al. Sparse autoencoders find highly interpretable features in language models. *arXiv preprint arXiv:2309.08600*, 2023.

Devlin, J., Chang, M.-W., Lee, K., and Toutanova, K. Bert: Pre-training of deep bidirectional transformers for language understanding, 2019. URL <https://arxiv.org/abs/1810.04805>.

Dunefsky, J., Chlenski, P., and Nanda, N. Transcoders find interpretable llm feature circuits, 2024. URL <https://arxiv.org/abs/2406.11944>.

Elhage, N. et al. A mathematical framework for transformer circuits. *Transformer Circuits Thread*, 2021. URL <https://transformer-circuits.pub/2021/framework/index.html>.

Etxaniz, J., Azkune, G., Soroa, A., de Lacalle, O. L., and Artetxe, M. Do multilingual language models think better in english?, 2023. URL <https://arxiv.org/abs/2308.01223>.

Grattafiori, A., Dubey, A., Jauhri, A., Pandey, A., Kadian, A., Al-Dahle, A., Letman, A., Mathur, A., Schelten, A., Vaughan, A., Yang, A., Fan, A., Goyal, A., Hartshorn, A., Yang, A., Mitra, A., Sravankumar, A., Korenev, A., Hinsvark, A., Rao, A., Zhang, A., Rodriguez, A., Gregerson, A., Spataru, A., Roziere, B., Biron, B., Tang, B., Chern, B., Caucheteux, C., Nayak, C., Bi, C., Marra, C., McConnell, C., Keller, C., Touret, C., Wu, C., Wong, C., Ferrer, C. C., Nikolaidis, C., Allonsius, D., Song, D., Pintz, D., Livshits, D., Wyatt, D., Esiobu, D., Choudhary, D., Mahajan, D., Garcia-Olano, D., Perino, D., Hupkes, D., Lakomkin, E., AlBadawy, E., Lobanova, E., Dinan, E., Smith, E. M., Radenovic, F., Guzmán, F., Zhang, F., Synnaeve, G., Lee, G., Anderson, G. L., Thattai, G., Nail, G., Mialon, G., Pang, G., Cucurell, G., Nguyen, H., Korevaar, H., Xu, H., Touvron, H., Zarov, I., Ibarra, I. A., Kloumann, I., Misra, I., Evtimov, I., Zhang, J., Copet, J., Lee, J., Geffert, J., Vranes, J., Park, J., Mahadeokar, J., Shah, J., van der Linde, J., Billock, J., Hong, J., Lee, J., Fu, J., Chi, J., Huang, J., Liu, J., Wang, J., Yu, J., Bitton, J., Spisak, J., Park, J., Rocca, J., Johnstun, J., Saxe, J., Jia, J., Alwala, K. V., Prasad, K., Upasani, K., Plawiak, K., Li, K., Heafield, K., Stone, K., El-Arini, K., Iyer, K., Malik, K., Chiu, K., Bhalla, K., Lakhotia, K., Rantala-Yeary, L., van der Maaten, L., Chen, L., Tan, L., Jenkins, L., Martin, L., Madaan, L., Malo, L., Blecher, L., Landzaat, L., de Oliveira, L., Muzzi, M., Pasupuleti, M., Singh, M., Paluri, M., Kardas, M., Tsimpoukelli, M., Oldham, M., Rita, M., Pavlova, M., Kambadur, M., Lewis, M., Si, M., Singh, M. K., Hassan, M., Goyal, N., Torabi, N., Bashlykov, N., Bogoychev, N., Chatterji, N., Zhang, N., Duchenne, O., Çelebi, O., Alrassy, P., Zhang, P., Li, P., Vasic, P., Weng, P., Bhargava, P., Dubal, P., Krishnan, P., Koura, P. S., Xu, P., He, Q., Dong, Q., Srinivasan, R., Ganapathy, R., Calderer, R., Cabral, R. S., Stojnic, R., Raileanu, R., Maheswari, R., Girdhar, R., Patel, R., Sauvestre, R., Polidoro, R., Sumbaly, R., Taylor, R., Silva, R., Hou, R., Wang, R., Hosseini, S., Chennabasappa, S., Singh, S., Bell, S., Kim, S. S., Edunov, S., Nie, S., Narang, S., Raparthy, S., Shen, S., Wan, S., Bhosale, S., Zhang, S., Vandenhende, S., Batra, S., Whitman, S., Sootla, S., Collot, S., Gururangan, S., Borodinsky, S., Herman, T., Fowler, T., Sheasha, T., Georgiou, T., Scialom, T., Speckbacher, T., Mihaylov, T., Xiao, T., Karn, U., Goswami, V., Gupta, V., Ramanathan, V., Kerkez, V., Gonguet, V., Do, V., Vogeti, V., Albiero, V., Petrovic, V., Chu, W., Xiong, W., Fu, W., Meers, W., Martinet, X., Wang, X., Wang,

X., Tan, X. E., Xia, X., Xie, X., Jia, X., Wang, X., Goldschlag, Y., Gaur, Y., Babaei, Y., Wen, Y., Song, Y., Zhang, Y., Li, Y., Mao, Y., Coudert, Z. D., Yan, Z., Chen, Z., Papakipos, Z., Singh, A., Srivastava, A., Jain, A., Kelsey, A., Shajnfeld, A., Gangidi, A., Victoria, A., Goldstand, A., Menon, A., Sharma, A., Boesenberg, A., Baevski, A., Feinstein, A., Kallet, A., Sangani, A., Teo, A., Yunus, A., Lupu, A., Alvarado, A., Caples, A., Gu, A., Ho, A., Poulton, A., Ryan, A., Ramchandani, A., Dong, A., Franco, A., Goyal, A., Saraf, A., Chowdhury, A., Gabriel, A., Bharambe, A., Eisenman, A., Yazdan, A., James, B., Maurer, B., Leonhardi, B., Huang, B., Loyd, B., Paola, B. D., Paranjape, B., Liu, B., Wu, B., Ni, B., Hancock, B., Wasti, B., Spence, B., Stojkovic, B., Gamido, B., Montalvo, B., Parker, C., Burton, C., Mejia, C., Liu, C., Wang, C., Kim, C., Zhou, C., Hu, C., Chu, C.-H., Cai, C., Tindal, C., Feichtenhofer, C., Gao, C., Civin, D., Beaty, D., Kreymer, D., Li, D., Adkins, D., Xu, D., Testuggine, D., David, D., Parikh, D., Liskovich, D., Foss, D., Wang, D., Le, D., Holland, D., Dowling, E., Jamil, E., Montgomery, E., Presani, E., Hahn, E., Wood, E., Le, E.-T., Brinkman, E., Arcaute, E., Dunbar, E., Smothers, E., Sun, F., Kreuk, F., Tian, F., Kokkinos, F., Ozgenel, F., Caggioni, F., Kanayet, F., Seide, F., Florez, G. M., Schwarz, G., Badeer, G., Swee, G., Halpern, G., Herman, G., Sizov, G., Guangyi, Zhang, Lakshminarayanan, G., Inan, H., Shojanazeri, H., Zou, H., Wang, H., Zha, H., Habeeb, H., Rudolph, H., Suk, H., Asperegn, H., Goldman, H., Zhan, H., Damlaj, I., Molybog, I., Tufanov, I., Leontiadis, I., Veliche, I.-E., Gat, I., Weissman, J., Geboski, J., Kohli, J., Lam, J., Asher, J., Gaya, J.-B., Marcus, J., Tang, J., Chan, J., Zhen, J., Reizenstein, J., Teboul, J., Zhong, J., Jin, J., Yang, J., Cummings, J., Carvill, J., Shepard, J., McPhie, J., Torres, J., Ginsburg, J., Wang, J., Wu, K., U., K. H., Saxena, K., Khandelwal, K., Zand, K., Matosich, K., Veeraraghavan, K., Michelena, K., Li, K., Jagadeesh, K., Huang, K., Chawla, K., Huang, K., Chen, L., Garg, L., A. L., Silva, L., Bell, L., Zhang, L., Guo, L., Yu, L., Moshkovich, L., Wehrstedt, L., Khabsa, M., Avalani, M., Bhatt, M., Mankus, M., Hasson, M., Lennie, M., Reso, M., Groshev, M., Naumov, M., Lathi, M., Keneally, M., Liu, M., Seltzer, M. L., Valko, M., Restrepo, M., Patel, M., Vyatskov, M., Samvelyan, M., Clark, M., Macey, M., Wang, M., Hermoso, M. J., Metanat, M., Rastegari, M., Bansal, M., Santhanam, N., Parks, N., White, N., Bawa, N., Singhal, N., Egebo, N., Usunier, N., Mehta, N., Laptev, N. P., Dong, N., Cheng, N., Chernoguz, O., Hart, O., Salpekar, O., Kalinli, O., Kent, P., Parekh, P., Saab, P., Balaji, P., Rittner, P., Bontrager, P., Roux, P., Dollar, P., Zvyagina, P., Ratanchandani, P., Yuvraj, P., Liang, Q., Alao, R., Rodriguez, R., Ayub, R., Murthy, R., Nayani, R., Mitra, R., Parthasarathy, R., Li, R., Hogan, R., Battey, R., Wang, R., Howes, R., Rinott, R., Mehta, S., Siby, S., Bondu, S. J., Datta, S., Chugh, S., Hunt, S., Dhillon, S., Sidorov, S., Pan, S., Mahajan, S., Verma, S., Yamamoto, S., Ramaswamy, S., Lindsay, S., Lindsay, S., Feng, S., Lin, S., Zha, S. C., Patil, S., Shankar, S., Zhang, S., Zhang, S., Wang, S., Agarwal, S., Sajuyigbe, S., Chintala, S., Max, S., Chen, S., Kehoe, S., Satterfield, S., Govindaprasad, S., Gupta, S., Deng, S., Cho, S., Virk, S., Subramanian, S., Choudhury, S., Goldman, S., Remez, T., Glaser, T., Best, T., Koehler, T., Robinson, T., Li, T., Zhang, T., Matthews, T., Chou, T., Shaked, T., Vontimitta, V., Ajayi, V., Montanez, V., Mohan, V., Kumar, V. S., Mangla, V., Ionescu, V., Poenaru, V., Mihailescu, V. T., Ivanov, V., Li, W., Wang, W., Jiang, W., Bouaziz, W., Constable, W., Tang, X., Wu, X., Wang, X., Wu, X., Gao, X., Kleinman, Y., Chen, Y., Hu, Y., Jia, Y., Qi, Y., Li, Y., Zhang, Y., Zhang, Y., Adi, Y., Nam, Y., Yu, Wang, Zhao, Y., Hao, Y., Qian, Y., Li, Y., He, Y., Rait, Z., DeVito, Z., Rosnbrick, Z., Wen, Z., Yang, Z., Zhao, Z., and Ma, Z. The llama 3 herd of models, 2024. URL <https://arxiv.org/abs/2407.21783>.

Hanna, M., Piotrowski, M., Lindsey, J., and Ameisen, E. circuit-tracer. <https://github.com/safety-research/circuit-tracer>, 2025. The first two authors contributed equally and are listed alphabetically.

Hoffmann, J., Borgeaud, S., Mensch, A., Buchatskaya, E., Cai, T., Rutherford, E., Casas, D. d. L., Hendricks, L. A., Welbl, J., Clark, A., et al. Training compute-optimal large language models. *arXiv preprint arXiv:2203.15556*, 2022.

Hu, J., Ruder, S., Siddhant, A., Neubig, G., Firat, O., and Johnson, M. Xtreme: A massively multilingual multi-task benchmark for evaluating cross-lingual generalization, 2020. URL <https://arxiv.org/abs/2003.11080>.

Huh, M., Cheung, B., Wang, T., and Isola, P. The platonic representation hypothesis, 2024. URL <https://arxiv.org/abs/2405.07987>.

Karpathy, A. NanoGPT. <https://github.com/karpathy/nanoGPT>, 2022.

Lample, G. and Conneau, A. Cross-lingual language model pretraining, 2019. URL <https://arxiv.org/abs/1901.07291>.

Lauscher, A., Ravishankar, V., Vulić, I., and Glavaš, G. From zero to hero: On the limitations of zero-shot cross-lingual transfer with multilingual transformers, 2020. URL <https://arxiv.org/abs/2005.00633>.

Lindsey, J., Ameisen, E., Nanda, N., Shabalin, S., Piotrowski, M., McGrath, T., Hanna, M., Lewis, O., Tigges, C., Merullo, J., Watts, C., Paulo, G., Batson, J., Gorton, L., Simon, E., Loeffler, M., McDougall, C., and Lin, J.

The circuits research landscape: Results and perspectives. *Neuronpedia*, 2025a. URL <https://neuronpedia.org/graph/info>.

Lindsey, J., Gurnee, W., Ameisen, E., Chen, B., Pearce, A., Turner, N. L., Citro, C., Abrahams, D., Carter, S., Hosmer, B., Marcus, J., Sklar, M., Templeton, A., Bricken, T., McDougall, C., Cunningham, H., Henighan, T., Jermyn, A., Jones, A., Persic, A., Qi, Z., Thompson, T. B., Zimmerman, S., Rivoire, K., Conerly, T., Olah, C., and Batson, J. On the biology of a large language model. *Transformer Circuits Thread*, 2025b. URL <https://transformer-circuits.pub/2025/attribution-graphs/biology.html>.

Merullo, J., Watts, C., Loeffler, M., Gorton, L., Simon, E., McGrath, T., and Lewis, O. Replicating circuit tracing for a simple known mechanism, June 2025. URL <https://www.goodfire.ai/research/replicating-circuit-tracing-for-a-simple-mechanism>. Accessed: 2025-10-07.

Meta AI. Llama-3.2-1b. <https://huggingface.co/meta-llama/Llama-3.2-1B>, 2026. Accessed: 2026-01-29.

Olah, C., Cammarata, N., Schubert, L., et al. Zoom in: An introduction to circuits. *Distill*, 2020. URL <https://distill.pub/2020/circuits/zoom-in/>.

Olsson, C. et al. In-context learning and induction heads. *Transformer Circuits*, 2022. URL <https://transformer-circuits.pub/2022/in-context-learning-and-induction-heads/index.html>.

Penedo, G., Kydlíček, H., Sabolčec, V., Messmer, B., Foroutan, N., Kargaran, A. H., Raffel, C., Jaggi, M., Werra, L. V., and Wolf, T. Fineweb2: One pipeline to scale them all — adapting pre-training data processing to every language. In *Second Conference on Language Modeling*, 2025. URL <https://openreview.net/forum?id=jnRBe6zatP>.

Pires, T., Schlinger, E., and Garrette, D. How multilingual is multilingual BERT? In Korhonen, A., Traum, D., and Márquez, L. (eds.), *Proceedings of the 57th Annual Meeting of the Association for Computational Linguistics*, pp. 4996–5001, Florence, Italy, July 2019. Association for Computational Linguistics. doi: 10.18653/v1/P19-1493. URL <https://aclanthology.org/P19-1493/>.

Saji, A., Husain, J. A., Jayakumar, T., Dabre, R., Kunchukuttan, A., and Puduppully, R. Romanlens: The role of latent romanization in multilinguality in llms, 2025. URL <https://arxiv.org/abs/2502.07424>.

Schut, L., Gal, Y., and Farquhar, S. Do multilingual llms think in english?, 2025. URL <https://arxiv.org/abs/2502.15603>.

Shi, F., Suzgun, M., Freitag, M., Wang, X., Srivats, S., Vosoughi, S., Chung, H. W., Tay, Y., Ruder, S., Zhou, D., et al. Language models are multilingual chain-of-thought reasoners. *arXiv preprint arXiv:2210.03057*, 2022.

Team, G., Riviere, M., Pathak, S., Sessa, P. G., Hardin, C., Bhupatiraju, S., Hussenot, L., Mesnard, T., Shahriari, B., Ramé, A., Ferret, J., Liu, P., Tafti, P., Friesen, A., Casbon, M., Ramos, S., Kumar, R., Lan, C. L., Jerome, S., Tsitsulin, A., Vieillard, N., Stanczyk, P., Girgin, S., Momchev, N., Hoffman, M., Thakoor, S., Grill, J.-B., Neyshabur, B., Bachem, O., Walton, A., Severyn, A., Parrish, A., Ahmad, A., Hutchison, A., Abdagic, A., Carl, A., Shen, A., Brock, A., Coenen, A., Laforge, A., Paterson, A., Bastian, B., Piot, B., Wu, B., Royal, B., Chen, C., Kumar, C., Perry, C., Welty, C., Choquette-Choo, C. A., Sinopalnikov, D., Weinberger, D., Vijaykumar, D., Rogozińska, D., Herbison, D., Bandy, E., Wang, E., Noland, E., Moreira, E., Senter, E., Eltyshev, E., Visin, F., Rasskin, G., Wei, G., Cameron, G., Martins, G., Hashemi, H., Klimczak-Plucińska, H., Batra, H., Dhand, H., Nardini, I., Mein, J., Zhou, J., Svensson, J., Stanway, J., Chan, J., Zhou, J. P., Carrasqueira, J., Iljazi, J., Becker, J., Fernandez, J., van Amersfoort, J., Gordon, J., Lipschultz, J., Newlan, J., yeong Ji, J., Mohamed, K., Badola, K., Black, K., Milligan, K., McDonell, K., Nguyen, K., Sodhia, K., Greene, K., Sjoesund, L. L., Usui, L., Sifre, L., Heuermann, L., Lago, L., McNealus, L., Soares, L. B., Kilpatrick, L., Dixon, L., Martins, L., Reid, M., Singh, M., Iverson, M., Görner, M., Velloso, M., Wirth, M., Davidow, M., Miller, M., Rahtz, M., Watson, M., Risdal, M., Kazemi, M., Moynihan, M., Zhang, M., Kahng, M., Park, M., Rahman, M., Khatwani, M., Dao, N., Bardoliwalla, N., Devanathan, N., Dumai, N., Chauhan, N., Wahltinez, O., Botarda, P., Barnes, P., Barham, P., Michel, P., Jin, P., Georgiev, P., Culliton, P., Kuppala, P., Comanescu, R., Merhej, R., Jana, R., Rokni, R. A., Agarwal, R., Mullins, R., Saadat, S., Carthy, S. M., Cogan, S., Perrin, S., Arnold, S. M. R., Krause, S., Dai, S., Garg, S., Sheth, S., Ronstrom, S., Chan, S., Jordan, T., Yu, T., Eccles, T., Hennigan, T., Kociský, T., Doshi, T., Jain, V., Yadav, V., Meshram, V., Dharmadhikari, V., Barkley, W., Wei, W., Ye, W., Han, W., Kwon, W., Xu, X., Shen, Z., Gong, Z., Wei, Z., Cotruta, V., Kirk, P., Rao, A., Giang, M., Peran, L., Warkentin, T., Collins, E., Barral, J., Ghahramani, Z., Hadsell, R., Sculley, D., Banks, J., Dragan, A., Petrov, S., Vinyals, O., Dean, J., Hassabis, D., Kavukcuoglu, K., Farabet, C., Buchatskaya, E., Borgeaud, S., Fiedel, N., Joulin, A., Kenealy, K., Dadashi, R., and Andreev, A. Gemma 2: Improving

open language models at a practical size, 2024. URL <https://arxiv.org/abs/2408.00118>.

Templeton, A., Conerly, T., Marcus, J., Lindsey, J., Bricken, T., Chen, B., Pearce, A., Citro, C., Ameisen, E., Jones, A., Cunningham, H., Turner, N. L., McDougall, C., MacDiarmid, M., Freeman, C. D., Sumers, T. R., Rees, E., Batson, J., Jermyn, A., Carter, S., Olah, C., and Henighan, T. Scaling monosemanticity: Extracting interpretable features from claude 3 sonnet. *Transformer Circuits Thread*, 2024. URL <https://transformer-circuits.pub/2024/scaling-monosemanticity/index.html>.

Touvron, H., Lavril, T., Izacard, G., Martinet, X., Lachaux, M.-A., Lacroix, T., Rozière, B., Goyal, N., Hambro, E., Azhar, F., Rodriguez, A., Joulin, A., Grave, E., and Lample, G. Llama: Open and efficient foundation language models, 2023. URL <https://arxiv.org/abs/2302.13971>.

Vatsal, S., Dubey, H., and Singh, A. Multilingual prompt engineering in large language models: A survey across nlp tasks, 2025. URL <https://arxiv.org/abs/2505.11665>.

Wang, K., Variengien, A., Conmy, A., Shlegeris, B., and Steinhardt, J. Interpretability in the wild: a circuit for indirect object identification in gpt-2 small, 2022. URL <https://arxiv.org/abs/2211.00593>.

Wei, J., Wang, X., Schuurmans, D., Bosma, M., Ichter, B., Xia, F., Chi, E., Le, Q., and Zhou, D. Chain-of-thought prompting elicits reasoning in large language models, 2022.

Wendler, C., Veselovsky, V., Monea, G., and West, R. Do llamas work in english? on the latent language of multilingual transformers, 2024. URL <https://arxiv.org/abs/2402.10588>.

Workshop, B., Scao, T. L., Fan, A., Akiki, C., Pavlick, E., Ilić, S., Hesslow, D., Castagné, R., Luccioni, A. S., Yvon, F., Gallé, M., Tow, J., Rush, A. M., Biderman, S., Webson, A., Ammanamanchi, P. S., Wang, T., Sagot, B., Muenninghoff, N., del Moral, A. V., Ruwase, O., Bawden, R., Bekman, S., McMillan-Major, A., Beltagy, I., Nguyen, H., Saulnier, L., Tan, S., Suarez, P. O., Sanh, V., Laurençon, H., Jernite, Y., Launay, J., Mitchell, M., Raffel, C., Gokaslan, A., Simhi, A., Soroa, A., Aji, A. F., Alfassy, A., Rogers, A., Nitzav, A. K., Xu, C., Mou, C., Emezue, C., Klamm, C., Leong, C., van Strien, D., Adelani, D. I., Radev, D., Ponferrada, E. G., Levkovizh, E., Kim, E., Natan, E. B., Toni, F. D., Dupont, G., Kruszewski, G., Pistilli, G., Elsahar, H., Benyamina, H., Tran, H., Yu, I., Abdulmumin, I., Johnson, I., Gonzalez-Dios, I., de la Rosa, J., Chim, J., Dodge, J., Zhu, J., Chang, J., Frohberg, J., Tobing, J., Bhattacharjee, J., Almubarak, K., Chen, K., Lo, K., Werra, L. V., Weber, L., Phan, L., al-lal, L. B., Tanguy, L., Dey, M., Muñoz, M. R., Masoud, M., Grandury, M., Šaško, M., Huang, M., Coavoux, M., Singh, M., Jiang, M. T.-J., Vu, M. C., Jauhar, M. A., Ghaleb, M., Subramani, N., Kassner, N., Khamis, N., Nguyen, O., Espejel, O., de Gibert, O., Villegas, P., Henderson, P., Colombo, P., Amuok, P., Lhoest, Q., Harliman, R., Bommasani, R., López, R. L., Ribeiro, R., Osei, S., Pyysalo, S., Nagel, S., Bose, S., Muhammad, S. H., Sharma, S., Longpre, S., Nikpoor, S., Silberberg, S., Pai, S., Zink, S., Torrent, T. T., Schick, T., Thrush, T., Danchev, V., Nikoulina, V., Laippala, V., Lepercq, V., Prabhu, V., Alyafeai, Z., Talat, Z., Raja, A., Heinzerling, B., Si, C., Taşar, D. E., Salesky, E., Mielke, S. J., Lee, W. Y., Sharma, A., Santilli, A., Chaffin, A., Stiegler, A., Datta, D., Szczechla, E., Chhablani, G., Wang, H., Pandey, H., Strobel, H., Fries, J. A., Rozen, J., Gao, L., Sutawika, L., Bari, M. S., Al-shaibani, M. S., Manica, M., Nayak, N., Teehan, R., Albanie, S., Shen, S., Ben-David, S., Bach, S. H., Kim, T., Bers, T., Fevry, T., Neeraj, T., Thakker, U., Raunak, V., Tang, X., Yong, Z.-X., Sun, Z., Brody, S., Uri, Y., Tojarieh, H., Roberts, A., Chung, H. W., Tae, J., Phang, J., Press, O., Li, C., Narayanan, D., Bourfoune, H., Casper, J., Rasley, J., Ryabinin, M., Mishra, M., Zhang, M., Shoeybi, M., Peyrounette, M., Patry, N., Tazi, N., Sanseviero, O., von Platen, P., Cornette, P., Lavallée, P. F., Lacroix, R., Rajbhandari, S., Gandhi, S., Smith, S., Requena, S., Patil, S., Dettmers, T., Baruwa, A., Singh, A., Cheveleva, A., Ligozat, A.-L., Subramonian, A., Névéol, A., Lovering, C., Garrette, D., Tunuguntla, D., Reiter, E., Taktasheva, E., Voloshina, E., Bogdanov, E., Winata, G. I., Schoelkopf, H., Kalo, J.-C., Novikova, J., Forde, J. Z., Clive, J., Kasai, J., Kawamura, K., Hazan, L., Carpuat, M., Clinciu, M., Kim, N., Cheng, N., Serikov, O., Antverg, O., van der Wal, O., Zhang, R., Zhang, R., Gehrmann, S., Mirkin, S., Pais, S., Shavrina, T., Scialom, T., Yun, T., Limisiewicz, T., Rieser, V., Protasov, V., Mikhailov, V., Prusachatkun, Y., Belinkov, Y., Bamberger, Z., Kasner, Z., Rueda, A., Pestana, A., Feizpour, A., Khan, A., Faranak, A., Santos, A., Hevia, A., Unldreaj, A., Aghagol, A., Abdollahi, A., Tammour, A., HajiHosseini, A., Behroozi, B., Ajibade, B., Saxena, B., Ferrandis, C. M., McDuff, D., Contractor, D., Lansky, D., David, D., Kiela, D., Nguyen, D. A., Tan, E., Baylor, E., Ozoani, E., Mirza, F., Ononiwu, F., Rezanejad, H., Jones, H., Bhattacharya, I., Solaiman, I., Sedenko, I., Nejadgholi, I., Passmore, J., Seltzer, J., Sanz, J. B., Dutra, L., Samagaio, M., Elbadri, M., Mieskes, M., Gerchick, M., Akinlolu, M., McKenna, M., Qiu, M., Ghauri, M., Burynok, M., Abrar, N., Rajani, N., Elkott, N., Fahmy, N., Samuel, O., An, R., Kromann, R., Hao, R., Alizadeh, S., Shubber, S., Wang, S., Roy, S., Viguier, S., Le, T., Oyebade, T., Le, T., Yang, Y., Nguyen, Z., Kashyap, A. R., Palasciano, A., Callahan, A., Shukla, A., Miranda-

Escalada, A., Singh, A., Beilharz, B., Wang, B., Brito, C., Zhou, C., Jain, C., Xu, C., Fourrier, C., Periñán, D. L., Molano, D., Yu, D., Manjavacas, E., Barth, F., Fuhrmann, F., Altay, G., Bayrak, G., Burns, G., Vrabec, H. U., Bello, I., Dash, I., Kang, J., Giorgi, J., Golde, J., Posada, J. D., Sivaraman, K. R., Bulchandani, L., Liu, L., Shinzato, L., de Bykhovetz, M. H., Takeuchi, M., Pàmies, M., Castillo, M. A., Nezhurina, M., Sänger, M., Samwald, M., Cullan, M., Weinberg, M., Wolf, M. D., Mihaljevic, M., Liu, M., Freidank, M., Kang, M., Seelam, N., Dahlberg, N., Broad, N. M., Muellner, N., Fung, P., Haller, P., Chandrasekhar, R., Eisenberg, R., Martin, R., Canalli, R., Su, R., Su, R., Cahyawijaya, S., Garda, S., Deshmukh, S. S., Mishra, S., Kiblawi, S., Ott, S., Sang-aroonsiri, S., Kumar, S., Schweter, S., Bharati, S., Laud, T., Gigant, T., Kainuma, T., Kusa, W., Labrak, Y., Bajaj, Y. S., Venkatraman, Y., Xu, Y., Xu, Y., Xu, Y., Tan, Z., Xie, Z., Ye, Z., Bras, M., Belkada, Y., and Wolf, T. Bloom: A 176b-parameter open-access multilingual language model, 2023. URL <https://arxiv.org/abs/2211.05100>.

Zhu, W., Lv, Y., Dong, Q., Yuan, F., Xu, J., Huang, S., Kong, L., Chen, J., and Li, L. Extrapolating large language models to non-english by aligning languages, 2024. URL <https://openreview.net/forum?id=CaP3CByuLp>.

Supplementary Materials

Table of Contents

PART I: Additional Methodological Details	16
A Multilingual Model Training	16
A.1 Tokenization Strategy	16
A.2 Model Architectures and Training	16
B CLT Training	17
B.1 Training Configuration	17
B.2 Performance	18
C Additional Validation Loss Curves Under Data Imbalance	19
C.1 GPT2 Models	19
C.2 TinyStories Models	20
D Language Feature Analysis	21
D.1 Methodology and Definitions	21
D.2 Feature Overlap Results	21
PART II: Complementary Analyses	23
E Multilingual Score	23
F Shared Multilingual Space Independence from English Dominance	23
PART III: Case Studies	25
G Case Studies: Multilingual Circuits	25
G.1 Multilingual Circuits: U-shaped Entropy	25
G.2 Multilingual Circuits: Failure Modes	27
G.3 Intervention Validation	29
H Extended Task Analysis: Translation and Cultural Prompts	29
H.1 Translation Prompts	29
H.2 Cultural Context Prompts	29
I Why English Performs Better: A Case Study	29
I.1 Cluster Activation Analysis	29
I.2 Sub-tokenization Effects	30
PART IV: Model Diffing and Tokenizer Analysis	30
M Model Diffing: Additional Material	30
M.1 Multilinguality of Repair Features	30
M.2 Token Assembly in Early Layers	30
N Tokenizer Analysis: BPE Constraints on Multilingual Processing	30
N.1 Vocabulary Allocation: Cannibalization Testing	30
N.2 Morphological Coherence	30
N.3 Mechanistic Implications	31

A. Multilingual Model Training

A.1. Tokenization Strategy

All models employ a unified tokenization approach designed to eliminate tokenization-induced biases. We train a debiased BPE tokenizer on uniformly distributed five-language data, with each language contributing exactly the same number of tokens. The resulting vocabulary contains 119,547 tokens, ensuring balanced representation across languages and writing systems.

Tokenizer Training Protocol

- **Training Data:** Equal token counts per language (20% each)
- **Vocabulary Size:** 119,547 tokens
- **Algorithm:** Byte-Pair Encoding (BPE)
- **Special Tokens:** BOS (beginning of sentence), EOS (end of sentence), PAD (padding), UNK (unknown)

A.2. Model Architectures and Training

A.2.1. MODEL ARCHITECTURE SPECIFICATIONS

We train transformer models following two architectures to enable comparisons across model families and scales:

Component	GPT-2	TinyStories
Vocabulary Size	119,547	119,547
Embedding Dimension	768	768
FFN Inner Dimension	3072	3072
Attention Head Dim.	64	48
Dropout Rate	0.1	0.1
Layer Norm	Pre-LN	Pre-LN
Activation Function	GELU	GELU
Position Encoding	Learned	Learned
Context Length	1024	512

Table 2. Detailed architecture hyperparameters.

A.2.2. TRAINING SCALE AND COMPUTE OPTIMIZATION

Following Chinchilla scaling laws (Hoffmann et al., 2022), we compute optimal training data sizes in Table 3.

$$N_{\text{tokens}} = 20 \times N_{\text{parameters}} \quad (7)$$

Model	Tokens	Steps	FLOPs
GPT-2	3.55B	1.73M	3.8×10^{12}
TinyStories	1.37B	670K	5.6×10^{11}

Table 3. Compute-optimal training specs.

A.2.3. TRAINING IMPLEMENTATION

We use the nanoGPT codebase (Karpathy, 2022) for reproducible transformer training and use the hyperparameters presented in Table 4.

Parameter	Value	Parameter	Value
Optimizer	AdamW	Learning Rate	6e-4
β_1	0.9	β_2	0.95
Weight Decay	0.1	Gradient Clipping	1.0
Warmup Steps	2000	LR Schedule	Cosine linear warmup
Batch Size	64	Gradient Accumulation	8 steps
Effective Batch Size	512		

Table 4. Training hyperparameters (horizontal layout for one-column appendix).

Optimization Configuration

Training Infrastructure We train each model on 4xH100 80GB GPUs. Training is distributed using data parallelism with gradient synchronization, and we use mixed precision (FP16) with automatic loss scaling.

A.2.4. TRAINING DYNAMICS

Figures 11, 12 and 13 shows training and validation loss across English data proportions. Higher English proportions reduce English validation loss but can slightly degrade performance on other languages.

A.2.5. TRAINING PROCEDURE AND MODELS TRAINED

Each architecture is trained on all data mixtures: 20%, 50%, 70% and 90%. Furthermore, we train another model on non-English data (25% for each of Arabic, Chinese, German and French).

For comparative purposes, we also include a pre-trained LLaMA-3.2-1B (Meta AI, 2026) model alongside our custom-trained models.

B. CLTs training

B.1. Training Configuration

We report in Table 5, the hyper-parameters of the CLT training. We mostly follow Anthropic guidelines (Ameisen et al., 2025). This setup is similar across Tinystories, GPT-2, and Llama CLTs.

Parameter	Value	Parameter	Value
<i>Model Architecture</i>			
Input dimension (d_{in})	768	Latent dimension (d_{latent})	24,576
Expansion factor	32	Context size	16
<i>Training Hyperparameters</i>			
Learning rate	2×10^{-4}	Adam β_1 / β_2	0.9 / 0.999
Batch size (tokens)	1,024	LR warm-up steps	1,000
LR decay steps	3,749		
<i>Loss Coefficients</i>			
L0 coefficient	2.0	Optimal L0	10
Dead penalty coefficient	1×10^{-5}		
<i>JumpReLU Configuration</i>			
Bandwidth	1.0	Initial threshold	0.03
<i>Other</i>			
Seed	42	Precision	float32 (mixed)

Table 5. Training Configuration (horizontal layout for one-column appendix).

However, for the Llama CLT, we use less features, as we are limited by GPU size with an expansion factor of around 4. We use `torch.float32` for the training as well.

For all CLTs, we stop training when the L0 sparsity coefficient goes below 10 and Explained Variance is beyond 70%. At this point, we save the full model activations and then load them in random chunks from the dataset for training. The CLTs contain roughly $78 \times 768 \times 32 \times 768$ parameters, though for the LLaMA CLT we use fewer features (expansion factor = 4) due to GPU memory constraints. Replacement scores are consistently in the range 0.75–0.8, which aligns with expected reconstruction performance. For circuit extraction, attribution graphs are pruned to retain 80% of cumulative node scores and 85% of cumulative edge scores using the circuit-tracing library. Training is conducted over approximately 200M tokens and follows standard CLT guidelines (Ameisen et al., 2025).

B.2. Performance

We report the amount of dead features and the performance of the different models (TinyStories, GPT2, Llama-3.2-1B) CLTs in Figures 8, 9 and 10.

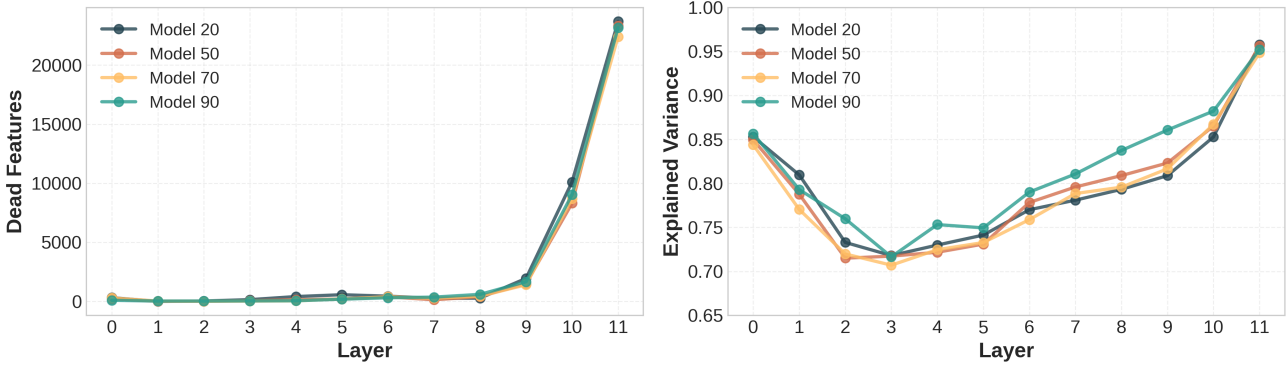


Figure 8. Dead feature count and explained variance across layers for the GPT-2 CLTs.

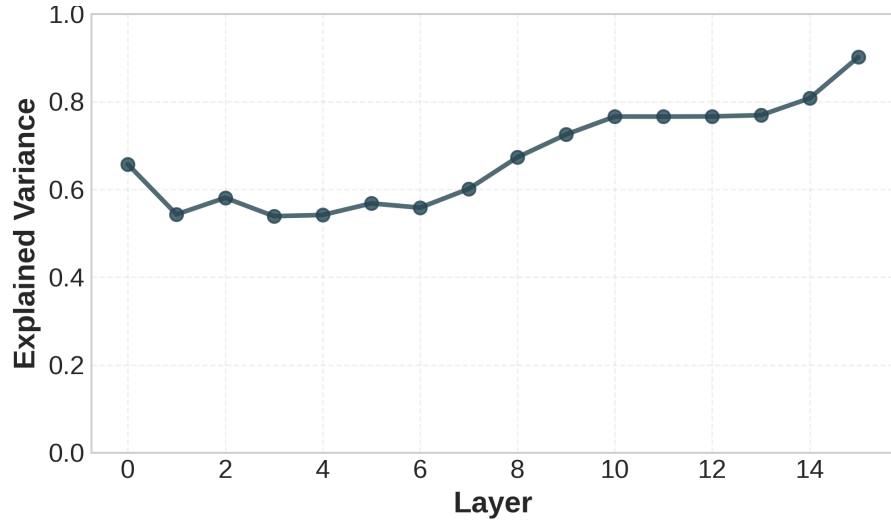


Figure 9. Explained variance over layers for the Llama CLT.

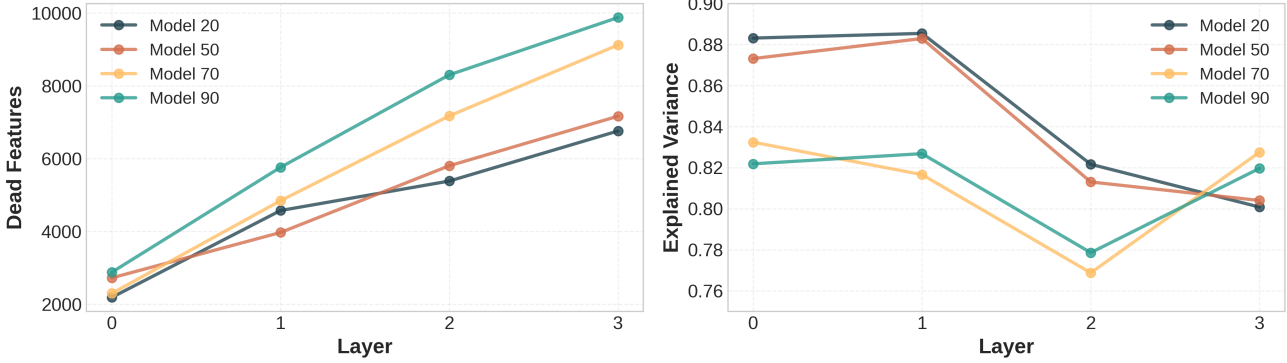


Figure 10. Dead feature count and explained variance across layers for the Tinstories CLTs.

C. Additional Validation Loss Curves Under Data Imbalance

C.1. GPT2-Models

In Section 4.1.1, we reported that the validation loss curves for the four non-English languages (Chinese, Arabic, German, French) show competitive performance. Here we show the curves.

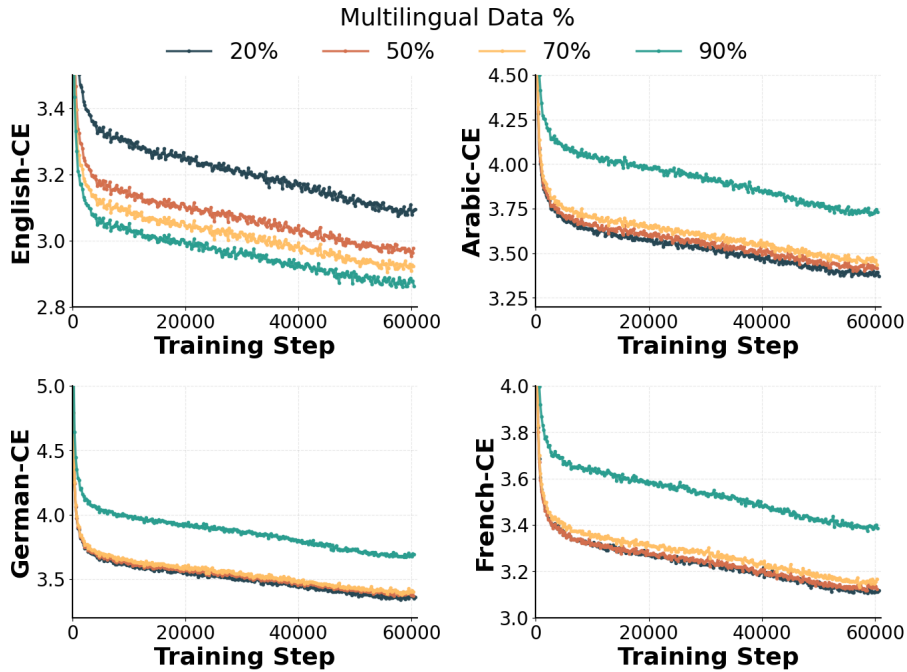


Figure 11. Validation cross-entropy loss curves for models trained on multilingual mixtures with varying proportions of English. Despite extreme imbalance (up to 90% English), the models maintain strong next-token prediction performance across languages.

We also provide additional results for Chinese. Figure 12 shows the validation loss curves for Chinese. The results mirror the patterns observed for other languages: despite extreme imbalance in the training data, the model maintains competitive prediction performance in Chinese, indicating that the robustness of multilingual circuits extends to typologically distinct languages.

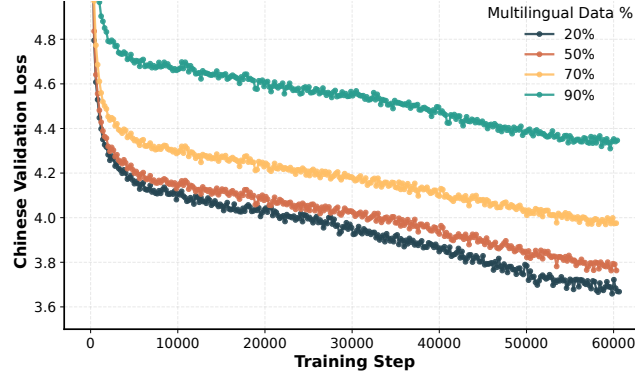


Figure 12. Validation cross-entropy loss curves for Chinese under varying proportions of English. The same robustness pattern holds as for other languages.

C.2. TinyStories Models

To assess whether the observed generalization dynamics also hold at small scale, we trained models on the **TinyStories** dataset. Figure 13 reports validation loss curves for five languages (English, Arabic, German, French, Chinese). Despite the reduced data scale and synthetic nature of TinyStories, the same trend emerges: performance remains robust across all languages, confirming that the organization of multilingual circuits is a stable property that persists across both large-scale and small-scale training regimes.

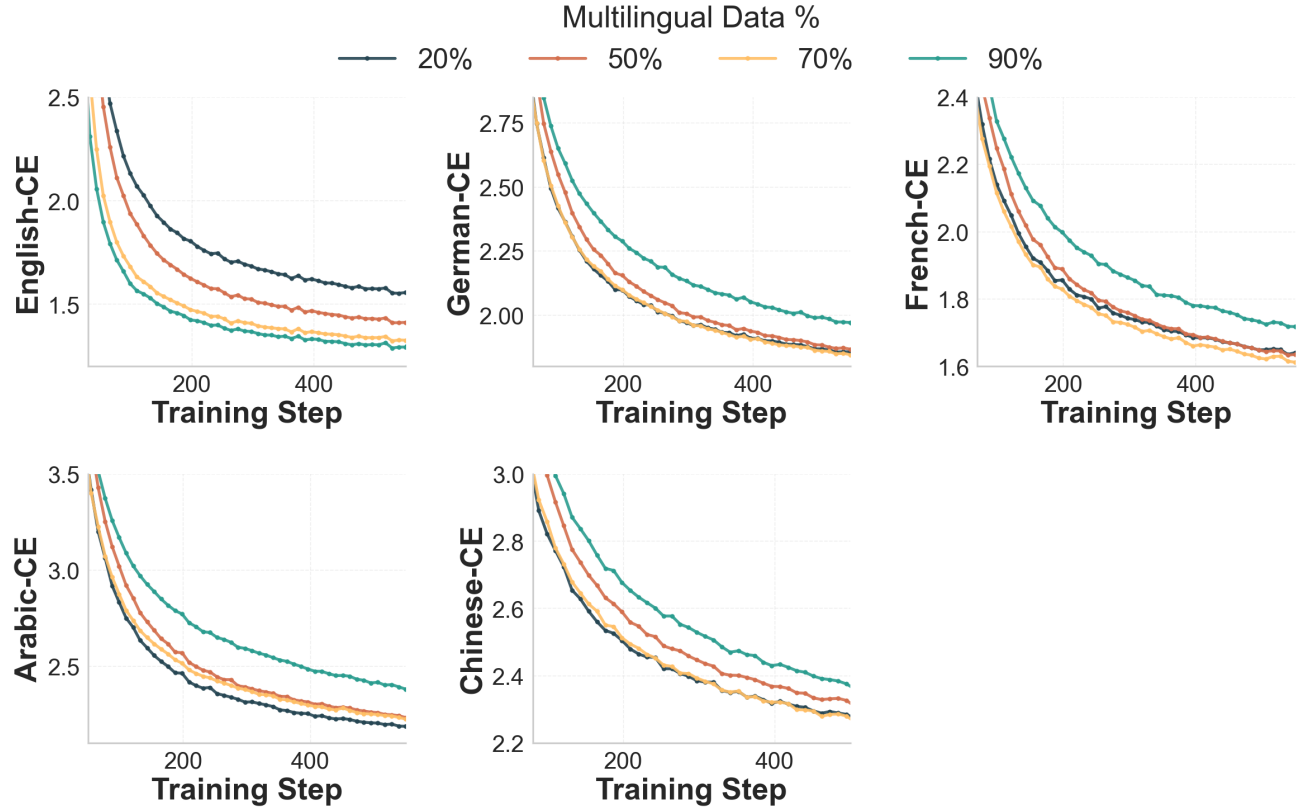


Figure 13. Validation cross-entropy loss curves for the **TinyStories-trained models** across five languages (English, Arabic, German, French, Chinese). Despite small-scale training data, models retain strong multilingual generalization under imbalance.

D. Language Feature Analysis

We analyze whether high-frequency features exhibit language specificity and quantify the extent to which language-specific features are shared across languages. This analysis uses precomputed activation statistics from CLT training with varying English proportions in the training data: 20%, 50%, 70%, and 90% English.

D.1. Methodology and Definitions

For each feature f at layer ℓ , we compute two statistics from the training data. First, the frequency $\text{freq}(f, \ell)$ represents the proportion of tokens for which the feature activates. Second, the language distribution $P(\text{lang} | f, \ell)$ captures the probability distribution over languages conditioned on feature activation. Specifically,

$$P(\text{lang} | f, \ell) = \frac{N_{\text{seq}}(f, \ell, \text{lang})}{N_{\text{seq}}(f, \ell, \text{total})},$$

where $N_{\text{seq}}(f, \ell, \text{lang})$ denotes the number of sequences in language lang in which feature f activates at least once.

To label a feature as language-specific, the feature must firstly be high-frequency, with $\text{freq}(f, \ell) \geq 0.03$. Second, the feature must be statistically associated with a given language, requiring $P(\text{lang} | f, \ell) \geq 0.5$, i.e., at least 50% of the sequences on which it activates are from that language. For example, a feature f at layer ℓ is labeled French-specific if both $\text{freq}(f, \ell) \geq 0.03$ and $P(\text{French} | f, \ell) \geq 0.5$.

For each language pair, we compute feature overlap via set intersection. Let

$$F_{\text{lang_a}} = \{(\ell, f) : \text{freq}(f, \ell) \geq 0.03 \wedge P(\text{lang_a} | f, \ell) \geq 0.5\}$$

denote the set of Language-A-specific features across all layers, with an analogous definition for $F_{\text{lang_b}}$. We define overlap as

$$\frac{|F_{\text{lang_a}} \cap F_{\text{lang_b}}|}{|F_{\text{lang_a}}|} \times 100\%,$$

D.2. Feature Overlap Results

Figure 14 shows the percentage of each non-English language’s language-specific features that overlap with English-specific features across the four training checkpoints. We observe a consistent increase in overlap as the proportion of English training data increases, rising from approximately 77% at 20% English to 84% at 90% English across all non-English languages. This trend indicates that increasing English exposure during training drives convergence toward an English-dominant feature space.

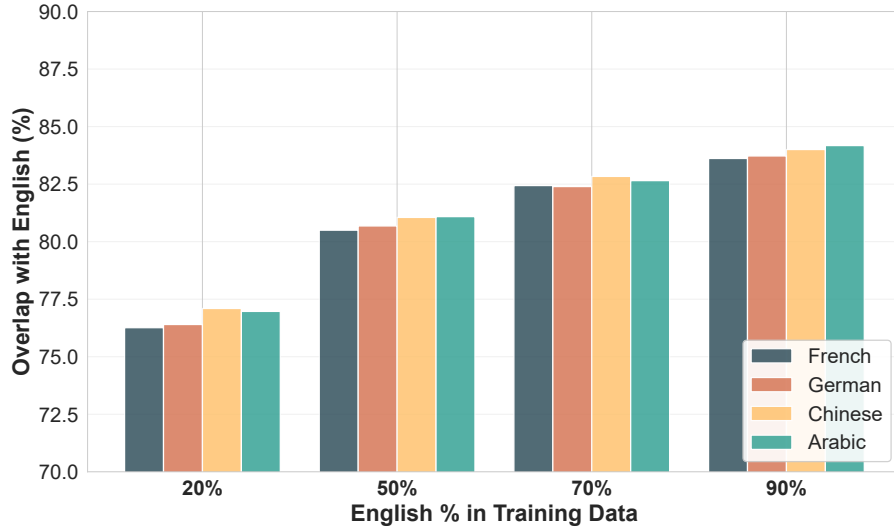


Figure 14. Overlap between non-English language-specific features and English-specific features across training checkpoints.

Figure 15 presents pairwise feature overlap among all non-English language pairs. We find that non-English languages overlap more strongly with each other (averaging 89% at 20% English) than they do with English (averaging 77% at 20% English), yielding a gap of approximately 12 percentage points. However, this gap progressively closes as English training proportion increases, reaching near parity at 90% English, indicating forced convergence.

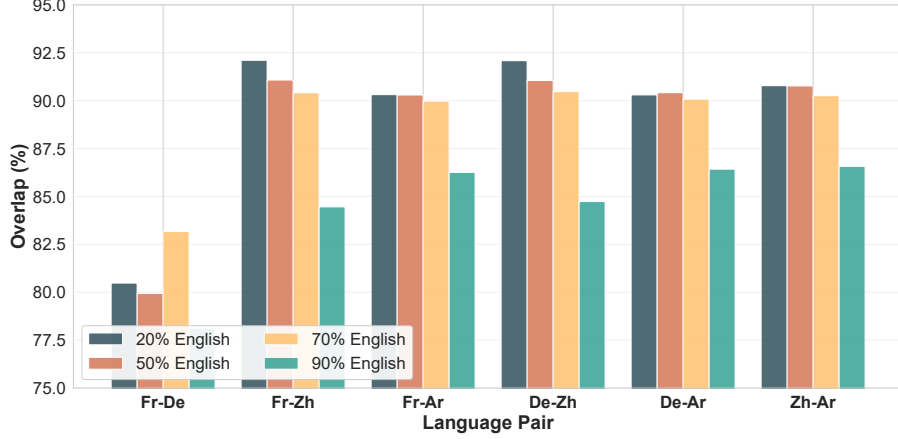


Figure 15. Pairwise overlap of language-specific features among non-English languages.

Figure 16 shows the full pairwise overlap matrix for the 90% English checkpoint as a heatmap. The visualization reveals notable asymmetries in pairwise relationships. For example, Chinese and Arabic maintain 86.6% overlap, substantially higher than the 78.1% overlap observed between French and German. All pairwise overlaps exceed 78%, confirming the existence of a broadly shared feature space. English exhibits relatively symmetric overlap with all other languages (83–84%), consistent with its role as a convergence point under high training proportions.

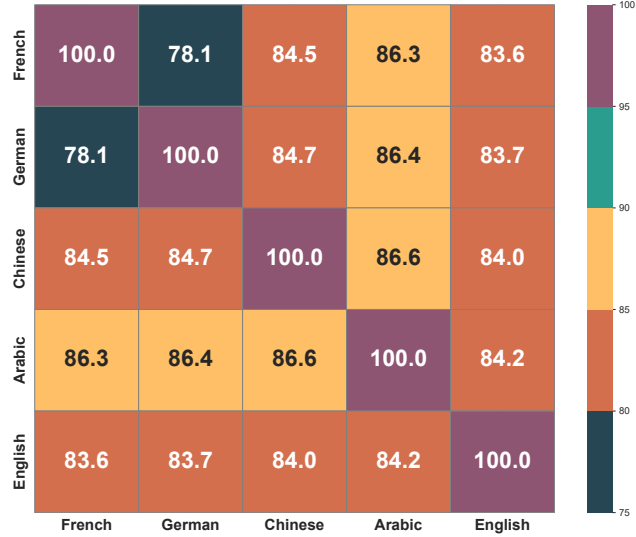


Figure 16. Complete pairwise feature overlap matrix at 90% English training.

We add here two plots related to the language features.

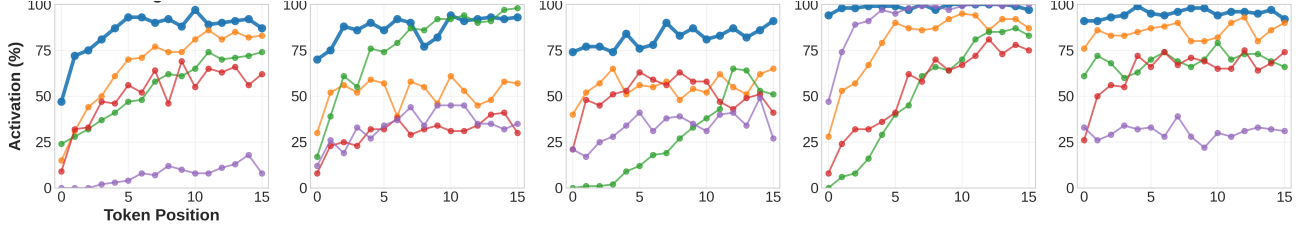


Figure 17. Activation rate over the top100 sequences of the language feature for the 20% model. We see that some language features are more active towards the end of the sequence. Highlighted is the language feature with the highest frequency.

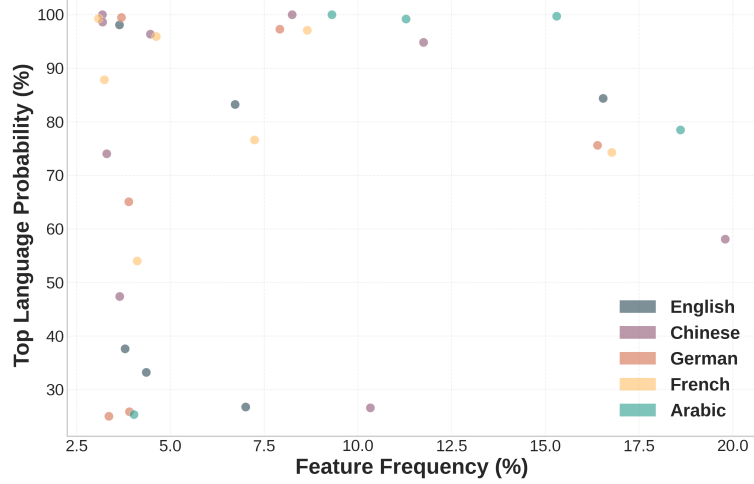


Figure 18. CLT features with the token activation frequency above 5% for the 20% model vs the probability in their top activating language. This shows that most high-frequency features are language features.

E. Multilingual Score

We compare the top100 multilingual score with the multilingual score computed over a large training subset (4M tokens)(Figure 19). Both entropy measures show the same overall trend across layers, with the top100 entropy consistently shifted toward lower values. The main difference appears in the earliest layers. This is likely because many features in these layers correspond to single-token activations, especially in layer 0. Given that the total number of features is limited to approximately 28K and multiple languages are involved, some features that mostly activate for a single token also tend to activate for other unrelated tokens.

Figure 19 also shows the frequency of the most activated token for each feature across the top100 sentences where that feature is strongest. We observe that in layer 0, and to a lesser extent in layers 1 and 2, most activations correspond to single tokens. For this reason, we decide to report the top100 score on the graphs.

We also report the general multilingual scores for Tinystories and Llama-3.2-1B in Figure 20.

During graph analysis, we display the multilingual score and the language distributions on a graph visual interface as shown in Figure 21.

F. Shared Multilingual Space Independence from English Dominance

To validate that the shared multilingual space structures do not require English dominance, we trained GPT-2 on balanced non-English data (25% French, 25% German, 25% Arabic, 25% Chinese) and computed weighted multilingual entropy across layers. The resulting curve exhibits the identical characteristic rise-and-fall pattern observed in English-dominant models, with peak entropy in layers 5–6 (Figure 22). This demonstrates that the shared multilingual space emergence is a fundamental architectural property, not an artifact of English dominance.

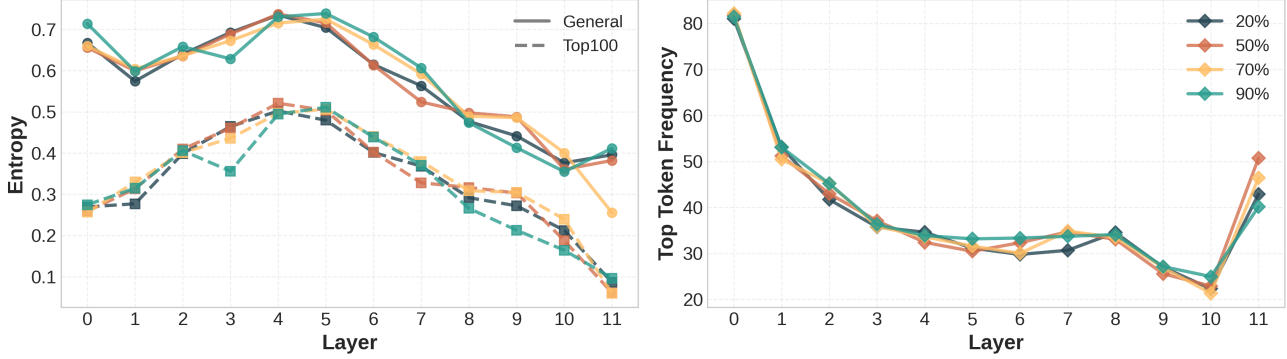


Figure 19. Comparison between the two multilingual entropy measures. One computed on the top100 activated sequences for each feature and one computed over a large training subset. On the right the frequency of activation of the most frequent token over the top100 sequences.

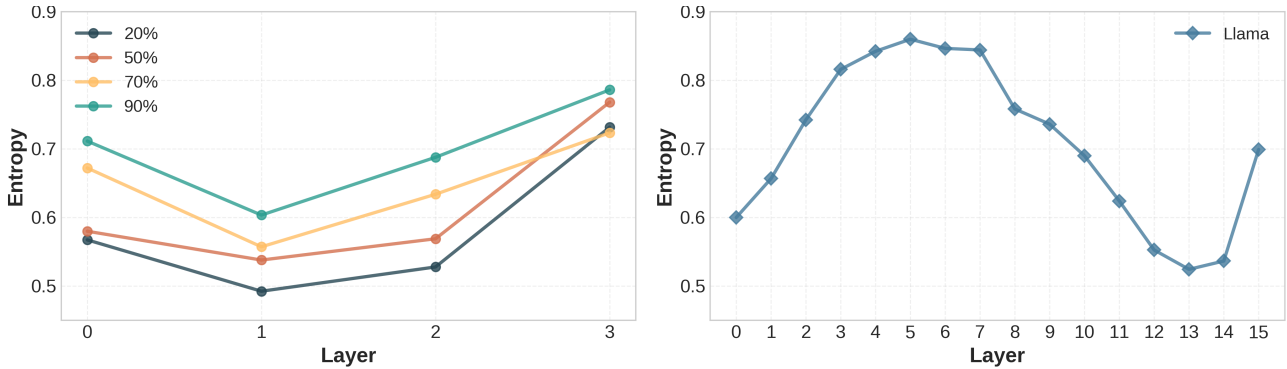


Figure 20. General multilingual score for the Tinystories model and Llama-3.2-1B. The final layer jump in the Llama CLT is potentially due to training dynamics. We find that the last layer has some features activated with small values that impact slightly the reconstruction performance but have a great impact on the multilingual score.

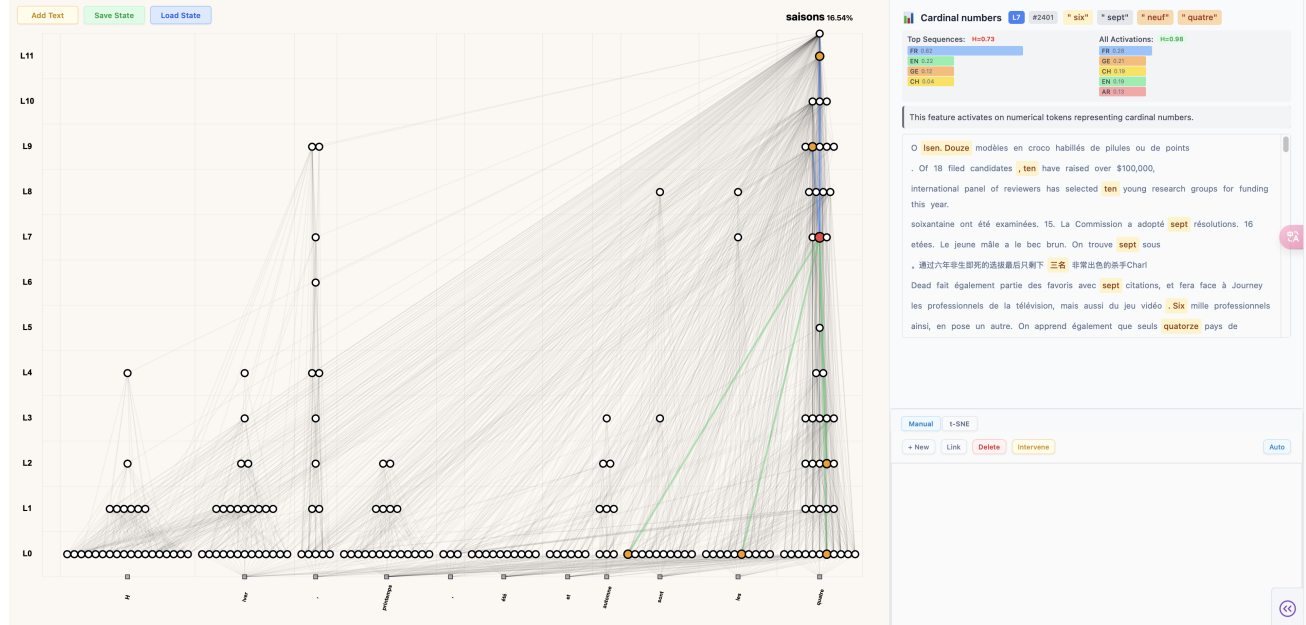


Figure 21. Graph visual interface with multilingual distributions and entropies on the top right.

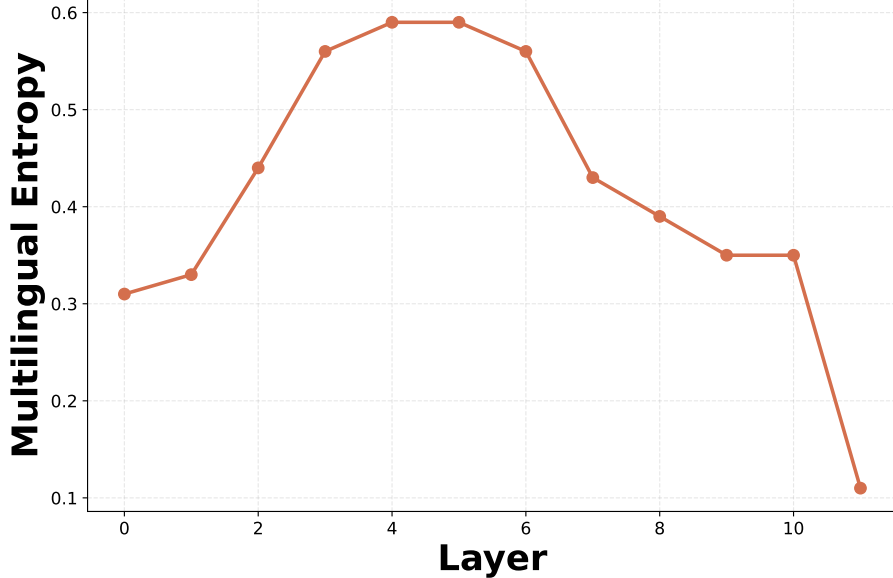


Figure 22. The Shared Multilingual Space emergence is independent of English dominance. Model trained without English (FR/DE/AR/ZH, 25% each) shows identical entropy curve to English-dominant model (20% EN + others), with characteristic rise-and-fall pattern and peak in layers 5–6.

G. Case Studies: Multilingual Circuits

Throughout this section, we present circuits to validate and visualize the findings discussed in the main text. Specifically, we organize our presentation as follows:

- i) Multilingual validation: We show circuits across additional tasks that support the multilingual shared space finding described in Section 4.1.3.
- ii) Failure cases and interventions: We provide examples of model failures and demonstrate that interventions on circuits—primarily those that strengthen existing internal features—can successfully guide the model to produce correct outputs. This completes Section 4.3.4
- iii) Translation and cultural prompts case study: We further validate our results with a case study on LLaMA-3.2-1B, using translation and culturally contextualized prompts, which confirms the robustness of our findings.

All examples produce clusters of circuits, which are manually constructed from features whose auto-interpretability descriptions and top-activating examples suggest similar functions. We further validate these clusters by intervening on them and confirming that the observed effects align with their interpreted descriptions.

G.1. Multilingual Circuits: U-shaped Entropy

In this appendix, we provide extended circuit visualizations complementing the analysis of Section 4.1.3. For each example, we extract attribution graphs across layers and present the identified circuits. Depending on the setting, each figure contains either (i) four subfigures, corresponding to the four training data mixtures (90%, 70%, 50% or 20% English), or (ii) five subfigures, corresponding to the five languages (English, Arabic, German, French, Chinese).

As observed in our main results, early and late layers predominantly encode language-specific circuits, while middle layers form clusters with high language entropy, reflecting multilingual representations. Exceptions arise for determinants and prepositions, whose circuits remain largely language-specific.

The top-right corner of each cluster shows its entropy score, defined as the average of the entropy values of the features it contains.

We now detail the examples analyzed.

G.1.1. PREPOSITION SENTENCES (ENGLISH: “It was a piece”)

We begin by analyzing English preposition prediction across training mixtures. Prepositions, being primarily functional rather than semantic, offer insight into the model’s handling of syntactic structures. In this case, we find that the model consistently relies on language-specific clusters.

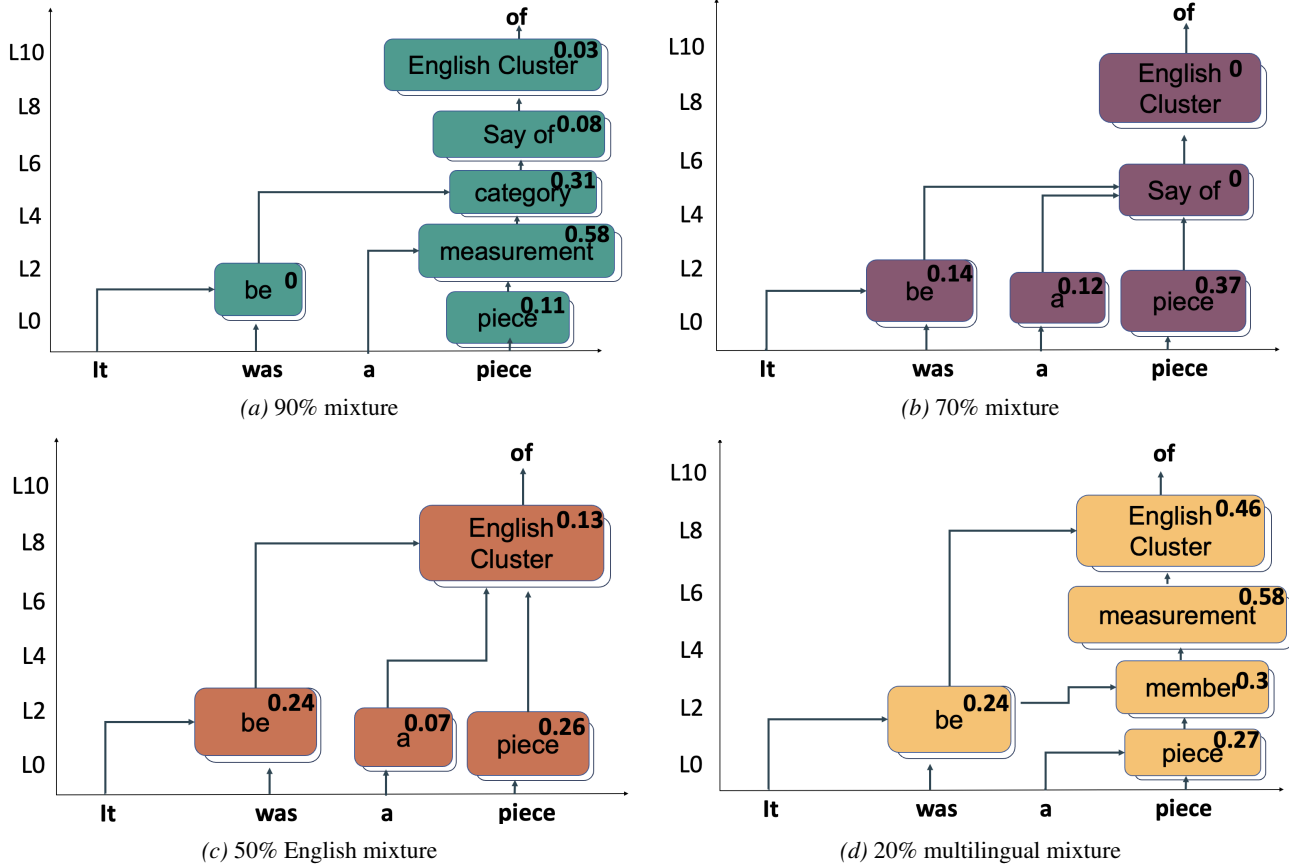


Figure 23. Circuits for English preposition prediction (“It was a piece”) across training mixtures.

G.1.2. PREPOSITION SENTENCES (FRENCH: “J’ai bu une tasse”)

We next examine French preposition prediction across the training mixtures. This setting tests whether the patterns observed for English prepositions generalize to another language.

G.1.3. CONTENT WORD SENTENCES (ENGLISH: “I prefer drinking tea to drinking”)

Next, we analyze content word prediction across languages in the 90% English mixture. Content words engage semantic and contextual representations, making them a strong testbed for cross-lingual generalization. We find robust multilingual clusters in middle layers across all five languages, even when trained under extreme imbalance.

G.1.4. CONTENT WORD SENTENCES: “Winter, spring, summer, and autumn are the four”

We analyze the prediction of content words in the sentence “Winter, spring, summer, and autumn are the four” across languages in the 20% English mixture. This example probes semantic and sequential reasoning across multiple languages, highlighting whether the model reuses internal circuits for similar content words. We find that middle layers consistently form multilingual clusters across all five languages, while early and late layers remain largely language-specific.

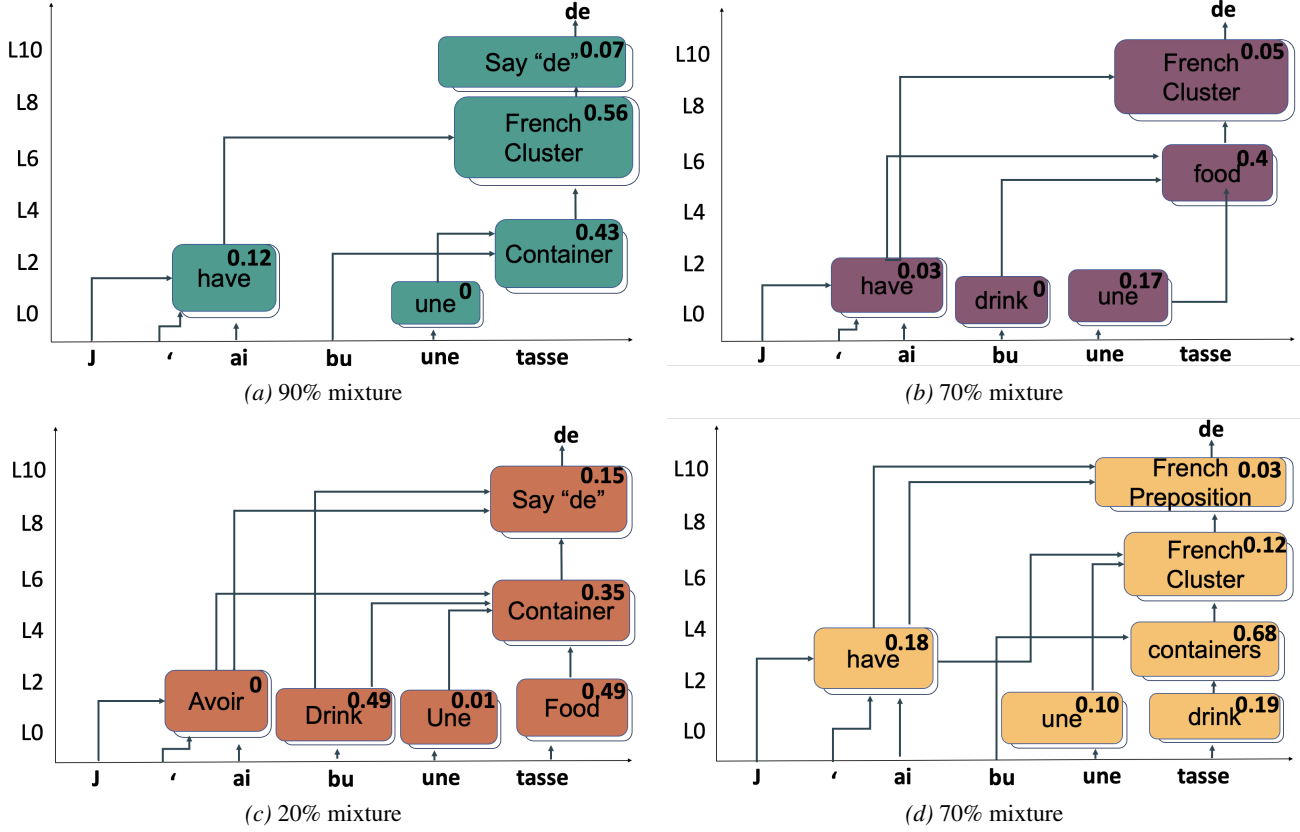


Figure 24. Circuits for French preposition prediction (“J’ai bu une tasse”) across training mixtures.

G.1.5. CALENDAR TERM PREDICTION (“Monday, Tuesday, Wednesday, Thursday”)

We study calendar term prediction across mixtures. Calendar terms primarily involve lexical memorization, providing a probe for multilingual circuit reuse. Across all mixtures, middle layers consistently form multilingual clusters, while early and late layers remain more language-specific.

G.1.6. ANALOGY SENTENCES (“the opposite of ‘men’ is ...”)

Finally, we analyze analogy-based prediction across mixtures. Unlike lexical recall, analogies engage relational reasoning. We find that the same multilingual clusters are reused across mixtures, especially in middle layers, underscoring their role in cross-lingual generalization.

G.2. Multilingual Circuits: Failure Modes

As discussed in Section 4.3, models trained on balanced data across languages still exhibit lower performance in non-English languages compared to English. To further support the findings from Section 4.3, we examine two tasks that probe distinct types of reasoning:

1. **Antonym Task:** Prompts such as The opposite of “men” is “” test semantic relations.
2. **Category Task:** Prompts like “Football, cycling, baseball are all” probe conceptual grouping.

We analyze five languages (English, German, French, Arabic, Chinese) across four training mixtures (20%, 50%, 70%, 90% English dominance) to uncover the mechanisms behind non-English failures.

G.2.1. ANTONYM TASK

Circuits driving antonym prediction are consistent across languages and mixtures, but their completeness depends on mixture balance. In Arabic under the 90% English mixture, the Men&Women cluster, present in most other languages, is missing but appears from the 50% mixture onward (Figure 29). Intervention experiments (Figure 34) confirm its causal role: adding this missing cluster restores correct Arabic predictions (Appendix G.3).

90% English Mixture Figure 30 shows circuit graphs for the antonym prompt “The opposite of “men” is “” across all five languages.

The circuits reveal why English achieves superior performance: languages that fail to predict the correct antonym consistently lack the Men&Woman cluster. Arabic shows particularly sparse connectivity, missing most multilingual clusters found in other languages due to limited circuit sharing with English.

70% English Mixture Figure 31 shows identical patterns: the Men&Women cluster remains absent where models fail. Only English sufficiently activates the reasoning circuit at this mixture level.

50% English Mixture Figure 32 validates previous patterns while showing increased presence of Men&Women clusters in non-English languages, reflecting the shift toward more uniform language distribution.

20% English Mixture Figure 33 shows more Men&Women clusters and improved performance, especially for Latin-script languages. Even at this balanced mixture, non-Latin script languages still demonstrate weaker circuit formation.

The circuit patterns suggest two competing mechanisms: a reasoning circuit that correctly predicts Women and a copying circuit that simply reproduces Men from the input tokens.

To validate these hypotheses, we conduct four investigations:

1. Intervention experiments: scale up reasoning circuit activation (Men&Women cluster) while scaling down copying circuit activation (Men cluster)
2. Comparative analysis across the three remaining mixtures to identify general trends
3. Activation value analysis of reasoning and copying circuits to validate insufficient activation hypothesis
4. Investigation of why English, German, and French demonstrate superior performance across all mixtures

G.2.2. CATEGORY COMPLETION TASK

We analyze the Category Completion task using the 20% mixture to understand performance in the balanced setting. Arabic performs poorly due to tokenization fragmentation, which forces early layers to reconstruct words rather than activate answer-related clusters. Intervention experiments (Figure 36) show that scaling these clusters restores correct predictions, emphasizing the importance of activation strength.

We present the circuits of the Category Completion Task presented in Figures 35.

We also present the intervention results for Arabic in Figure 36, the only language where the model failed.

Comparatively, English consistently triggers stronger responses in task-specific circuits (Men&Women for Antonym, Say Sports for Category Completion). This difference narrows under balanced mixtures but remains linked to sub-tokenization: languages with fragmented tokens show weaker edge strengths from embeddings to target clusters, partially explaining their reduced accuracy (Appendix I).

We further validate these mechanisms through more complex tasks (translation and cultural prompts on LLaMA-1B), tokenizer analysis, and quantitative validation across the attribution graphs (see Appendix H).

G.3. Intervention Validation

We define an **intervention on a cluster of circuits** as steering the residual stream using a vector constructed from the cluster's features. Specifically, let f_1, f_2, \dots, f_n denote the features in a cluster, and let $v(f_i)$ be the decoded vector of feature f_i . The intervention vector v_{int} is then given by

$$v_{\text{int}} = \alpha \sum_{i=1}^n v(f_i), \quad (8)$$

where α is a scaling factor determined via sweeping to optimize the effect of the intervention. The residual stream is updated by adding v_{int} at the relevant layer.

Figures 34, 37 and 36 demonstrate successful interventions that validate the competing circuits hypothesis.

In all the examples where the model fails to get the right answer, scaling up the reasoning circuit while scaling down the copying circuit consistently produces correct predictions. We sweep positive coefficients for the reasoning circuit (1 to 30) and negative coefficients for the copying circuit (-30 to -1) to determine optimal steering values.

Figures 33, 32, 31, and 30 further validate our hypothesis. In particular, most of the examples where the model fails to predict the correct answer show either an absence of the reasoning circuit or a low level of its activation, and this pattern becomes less pronounced as we move towards the 20% mixture. Taken together with the intervention results, this supports our hypothesis about circuit competition.

H. Extended Task Analysis: Translation and Cultural Prompts

We tested whether the shared multilingual space mechanisms generalize beyond simple lexical tasks (antonym, category completion) to more complex, context-dependent tasks on LLaMA-3.2-1B (Meta AI, 2026). Attribution analysis across all complex task circuits reveals the consistent three-phase structure: early layers extract language-specific features, middle layers form language-neutral semantic representations, and late layers activate language-specific output clusters.

H.1. Translation Prompts

Translation tasks require cross-lingual semantic mapping without explicit language labels:

- “English: Flower, Français: __”
- “English: Flower, Arabic: __”

Circuits maintain the same rise-and-fall pattern across layers, despite task complexity.

H.2. Cultural Context Prompts

Models complete: “The best dish is...” and generate language-appropriate food answers.

The same multilinguality pattern emerges across these circuits (see Figure 39).

I. Why English Performs Better: A Case Study

We present a case study examining the 20% mixture to understand performance disparities in balanced training.

I.1. Cluster Activation Analysis

We measure activation strength of task-relevant clusters across languages. For the Antonym task, we track the Man&Woman cluster; for Category Completion, the Say Sports cluster.

Figure 40 shows activation patterns. English consistently produces higher activations than other languages. This disparity decreases approaching the 20% mixture, suggesting balanced training mitigates but does not eliminate the advantage.

I.2. Sub-tokenization Effects

We quantify sub-tokenization impact by measuring edge strength from token embeddings to target clusters. Edge strength is the dot product between the residual stream after token embedding and the cluster’s input direction.

Figure 41 presents results across languages with varying sub-tokenization rates. Highly sub-tokenized languages (e.g., Arabic) show significantly weaker edge strengths. Fragmented tokens fail to properly activate downstream circuits—semantic information distributes across multiple sub-tokens rather than concentrating in a single embedding.

J. Model Diffing: Additional Material

J.1. Multilinguality of Repair Features

As mentioned in Section 4.3.2, we estimated the distribution of languages for features in each of our buckets. We evaluate on 10000 tokens and we report the scores in Figure 42

The blurred bars indicate features for which the language distribution could not be reliably estimated. Although we use a large number of tokens, some features are rarely activated, resulting in insufficient samples to accurately characterize their language distribution.

J.2. Token Assembly in Early Layers

Token assembly refers to the process by which early layers reconstruct sub-tokenized inputs (particularly fragmented words from morphologically rich languages like Arabic) into coherent higher-level representations before semantic processing. Logit Lens results, as described in Section 4.3.3, are shown in Figure 43. As observed, finetuning improves word assembly in Arabic and German. Counterintuitively, it increases fragmentation in Chinese, likely due to the comparatively high-rank updates required for Chinese. This suggests that the model relies more on memorization than on structured rules or heuristics for Chinese, as learning this language consumes a larger portion of the model’s capacity, leaving less capacity available for other languages.

K. Tokenizer Analysis: BPE Constraints on Multilingual Processing

Despite employing a debiased multilingual BPE tokenizer trained on balanced data, morphologically rich languages exhibit severe sub-tokenization compared to other languages. We isolate the source of this disparity through three complementary analyses.

K.1. Vocabulary Allocation: Cannibalization Testing

To rule out allocation bias, we computed fertility ratios (tokens per word) for language-specific tokenizers:

- Arabic: 1.06
- Chinese: 1.03
- English: 0.99
- French: 0.96
- German: 1.00

All ratios cluster near 1.0, confirming that the debiased tokenizer allocates vocabulary fairly across languages. The disparity in fragmentation therefore stems from linguistic properties, not allocation bias.

K.2. Morphological Coherence

Token-morpheme coherence (how well token boundaries align with morpheme boundaries) diverges dramatically:

Concrete examples illustrate this fragmentation:

Metric	Arabic	English
Token Fertility	1.97	1.53
Token-Morpheme Coherence	0.10	0.42
Meaningless Fragments (%)	89	58

Table 6. Arabic exhibits 4x lower morphological coherence than English despite fair vocabulary allocation. Meaningless fragments represent tokens that carry no semantic content.

- *al-radar* (radar) fragments into [*al-r*, *ad*, *ar*]: prefix, middle, and suffix separated
- *tafaqad* (inspect) fragments into [*taf*, *qad*]: broken across morpheme boundaries with subtokens having no meaning.

English maintains coherence: “reading” → [“read”, “ing”], preserving morpheme structure.

K.3. Mechanistic Implications

This tokenization constraint directly impacts early-layer processing. Fragmented tokens lack semantic content, forcing early layers (0–3) to first reconstruct word boundaries before processing meaning. This reconstruction cost weakens the initial activation patterns that propagate through multilingual circuits.

Critically, despite this early-layer handicap, Arabic still develops identical shared multilingual representations in middle layers (5–6), demonstrating that the shared multilingual space mechanism is robust to tokenization disadvantage. However, the initial signal degradation explains why Arabic exhibits weaker circuit activation and lower downstream performance despite mechanistic equivalence.

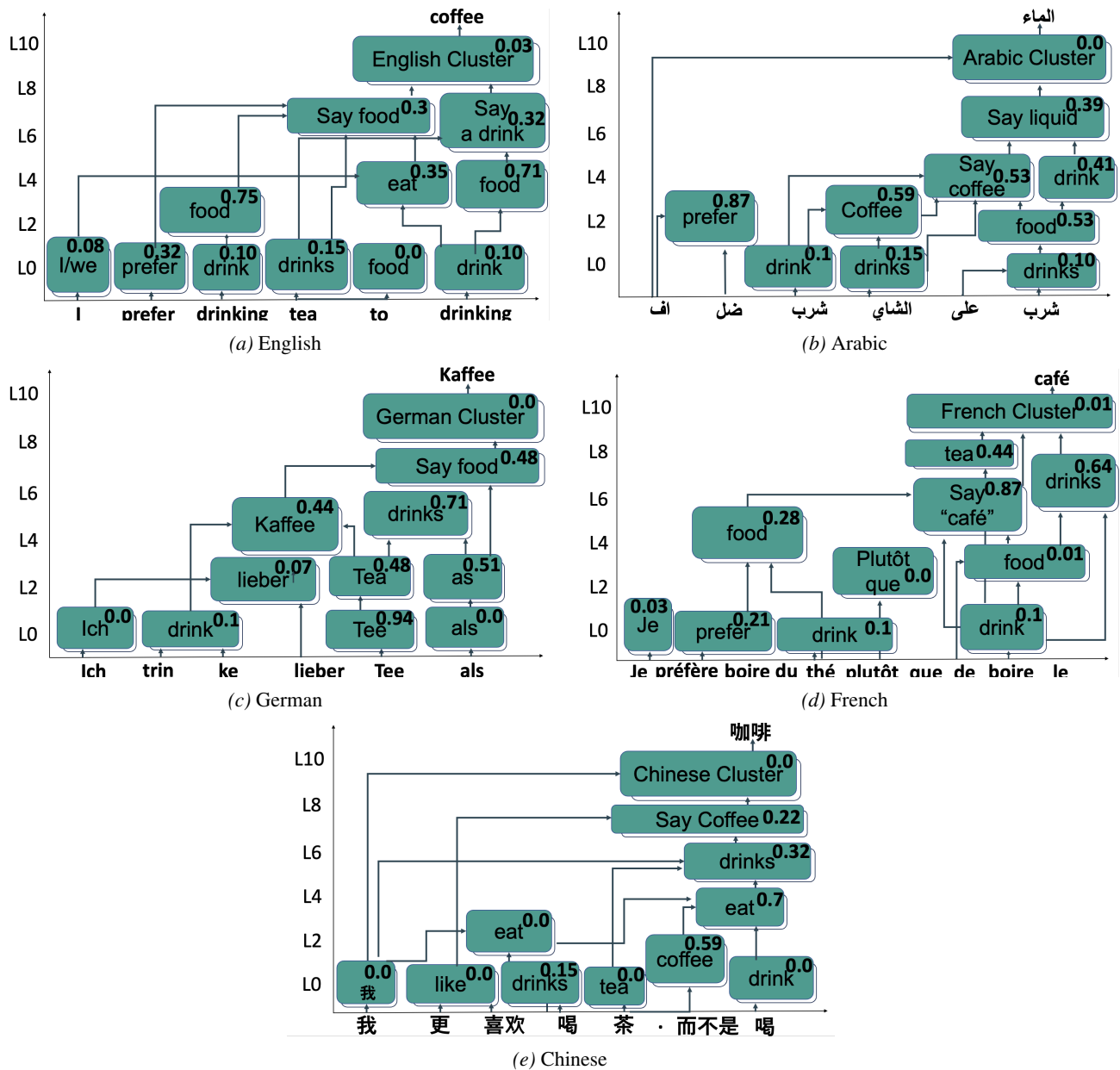


Figure 25. Circuits for content word prediction (“I prefer drinking tea to drinking”) across languages in the 90% English mixture.

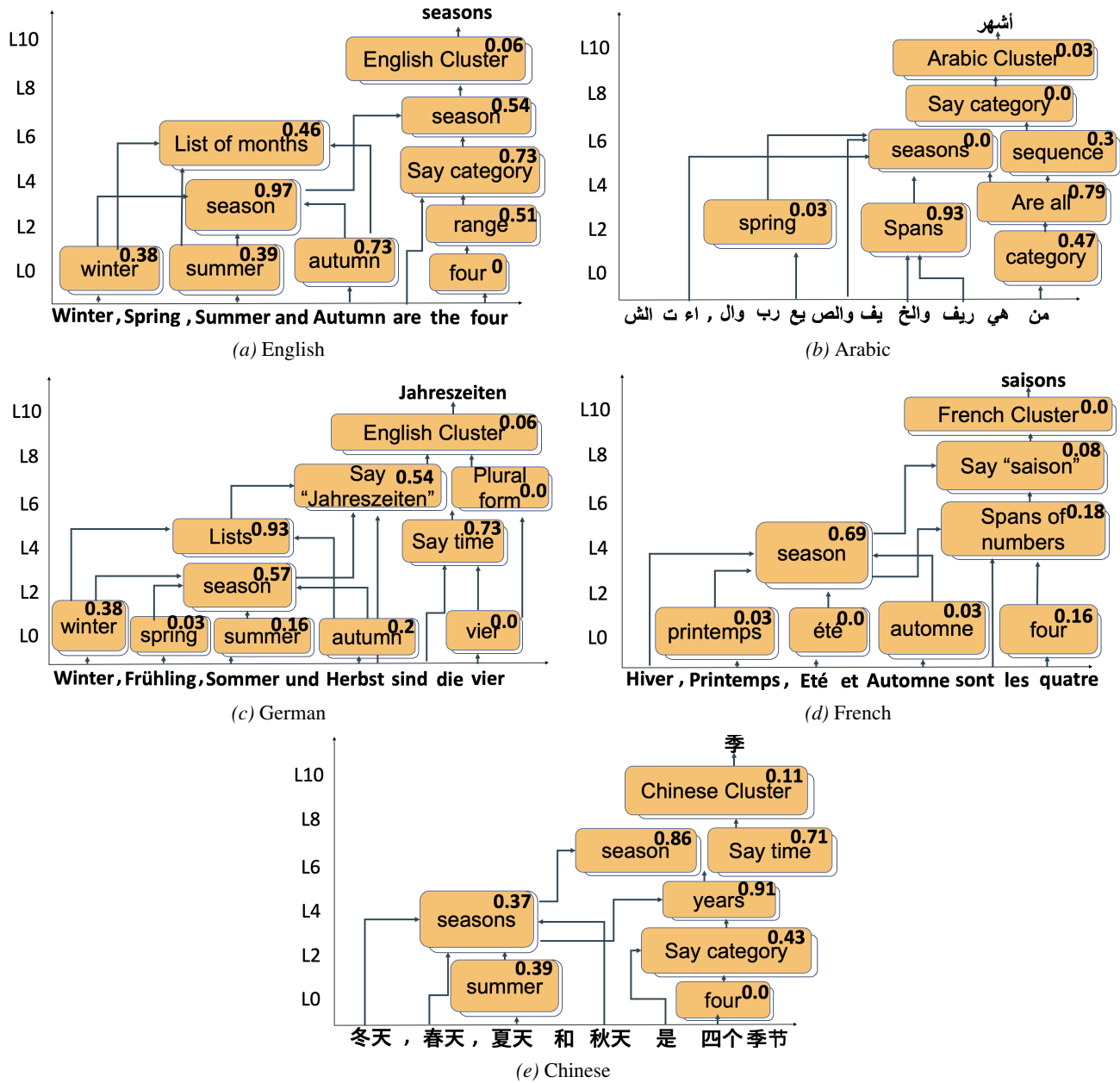


Figure 26. Circuits for content word prediction (“Winter, spring, summer, and autumn are the four”) across five languages in the 20% English mixture.

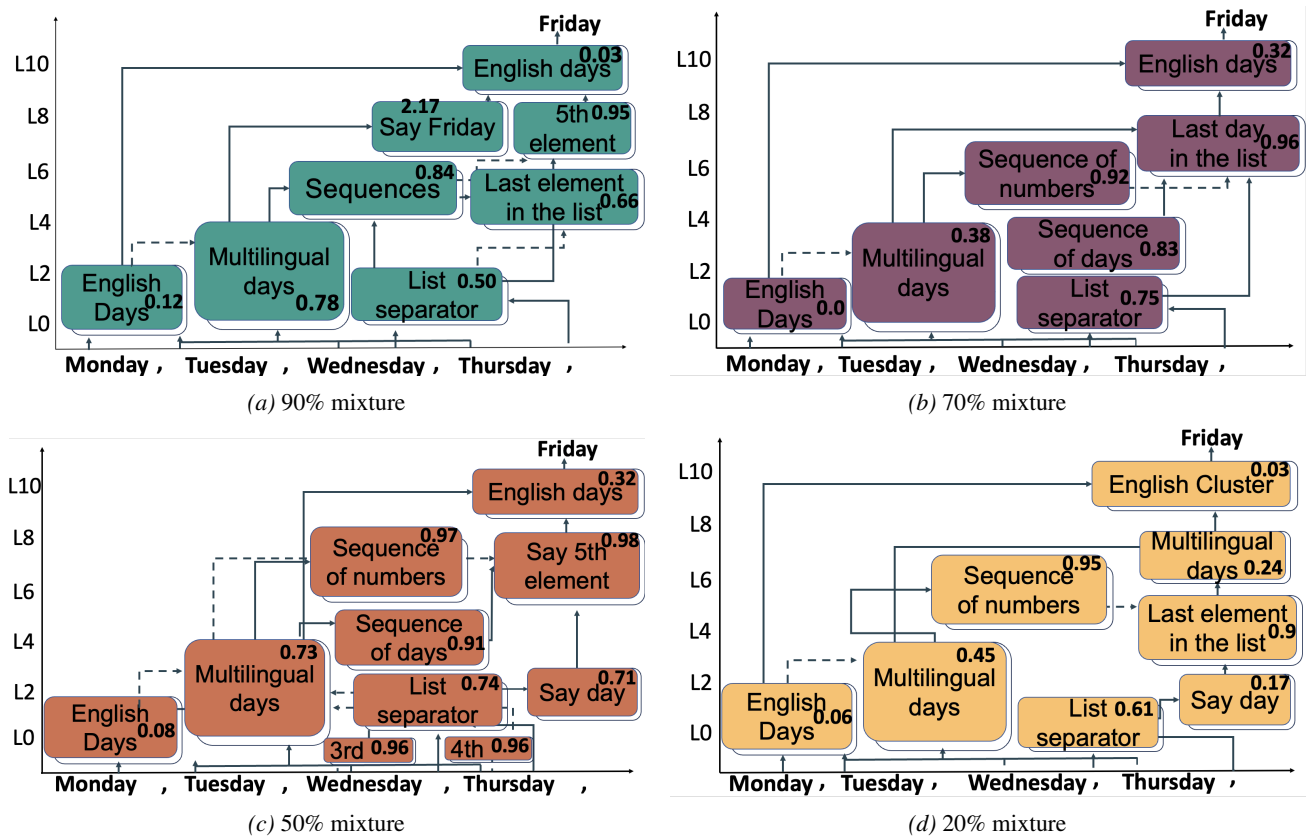


Figure 27. Circuits for calendar term prediction (“Monday, Tuesday, Wednesday, Thursday”) across mixtures.

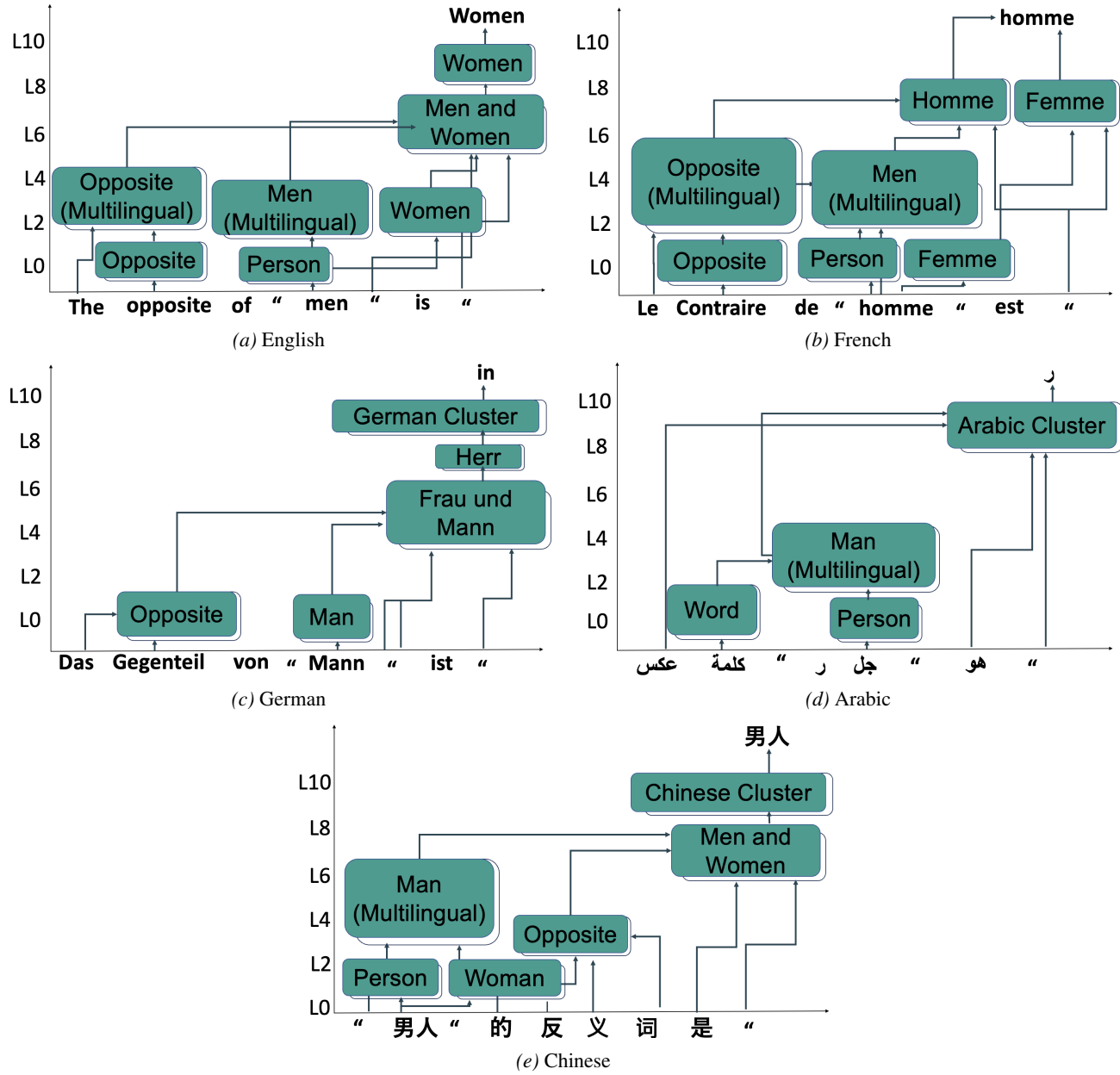


Figure 28. Circuits for analogy-based prediction (“the opposite of ‘men’ is ...”) across mixtures.

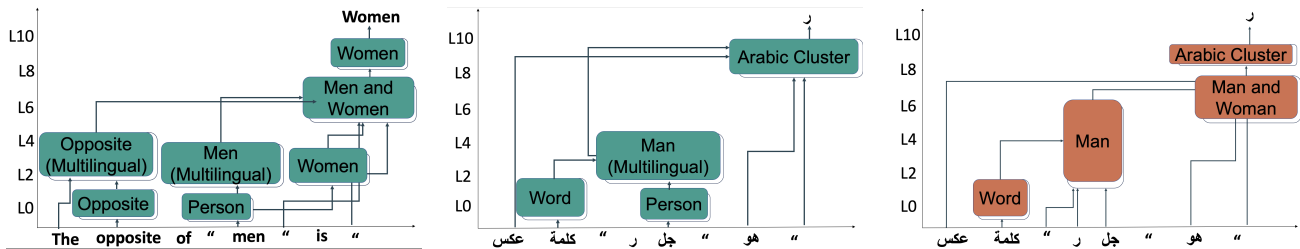


Figure 29. Circuit structures across language mixtures. Green: 90% English mixture, orange: 50% mixture. Key clusters missing in Arabic at 90% emerge by 50%, indicating mixture-dependent circuit formation. Additional examples appear in Appendix G.2.

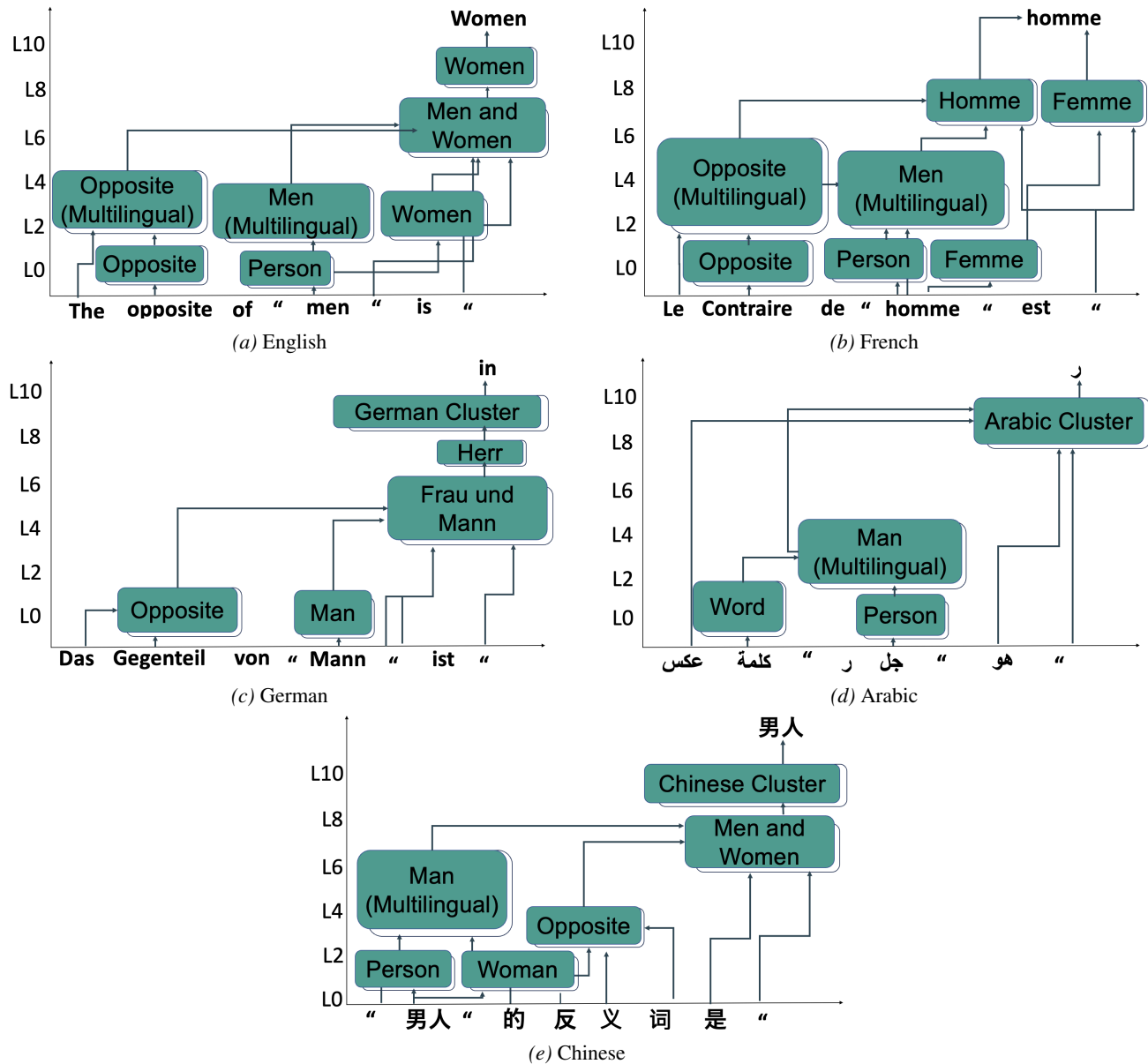


Figure 30. Circuits identified across five languages at 90% mixture.

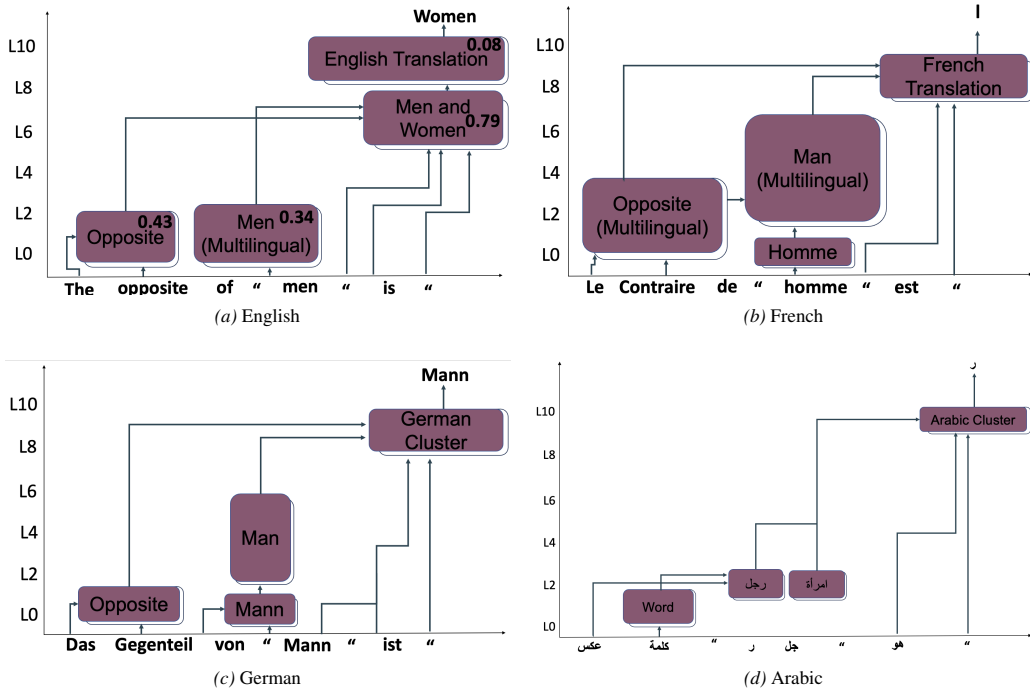


Figure 31. Circuits identified across five languages at 70% mixture.

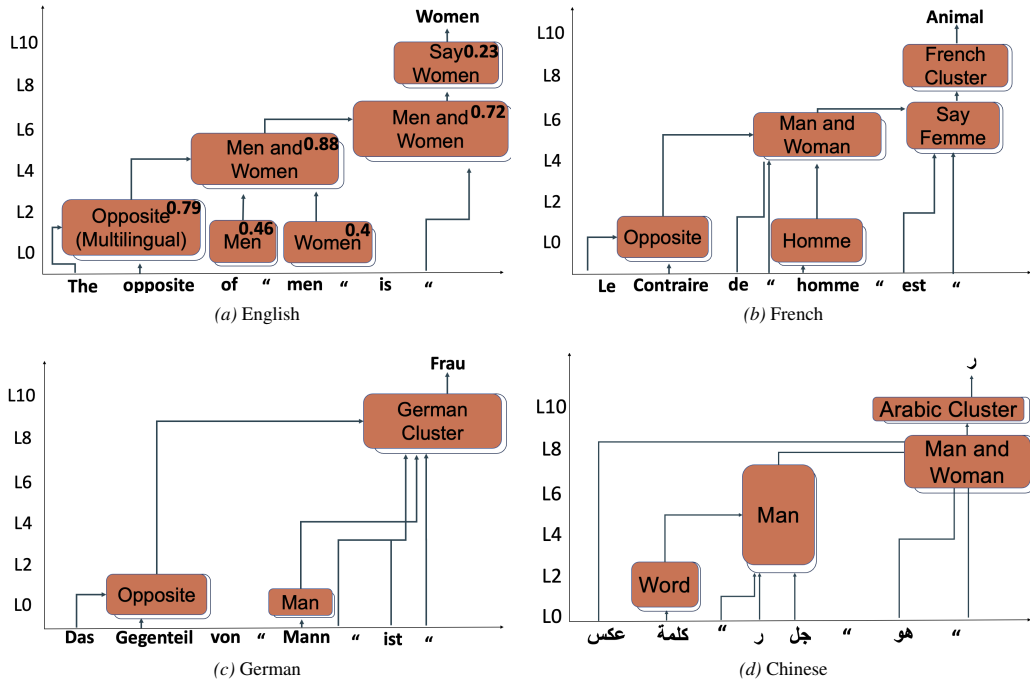


Figure 32. Circuits identified across five languages at 50% mixture.

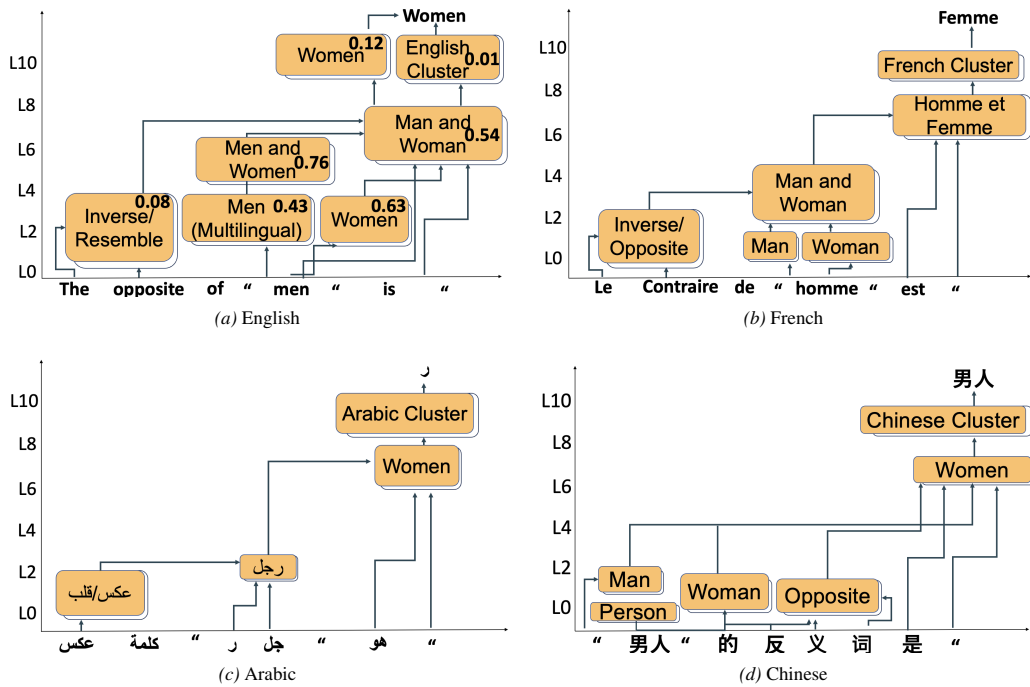


Figure 33. Circuits identified across five languages at 20% mixture.

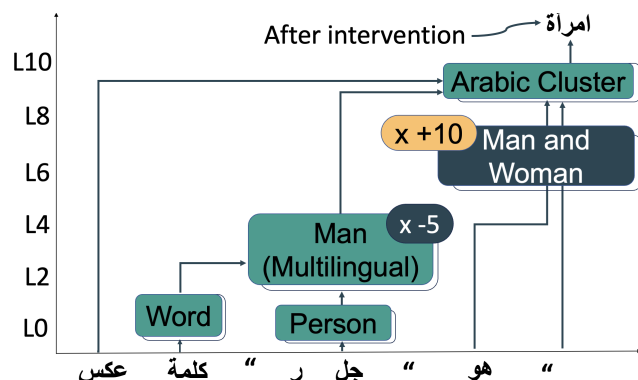


Figure 34. Adding the missing Men&Women cluster to the Arabic circuit restores performance.

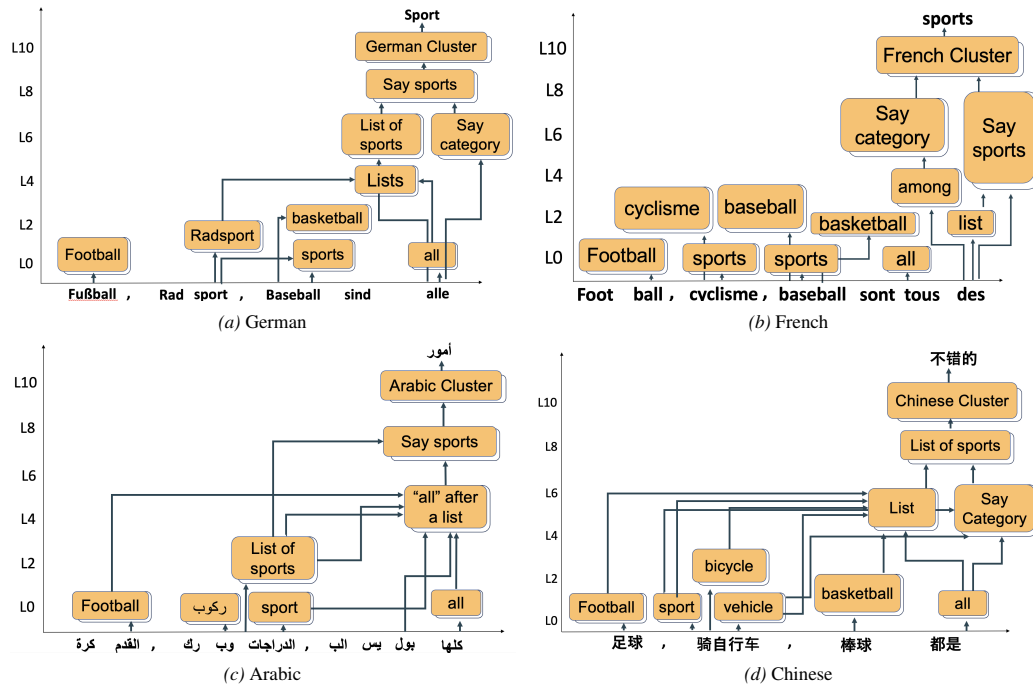


Figure 35. Circuits for category completion task.

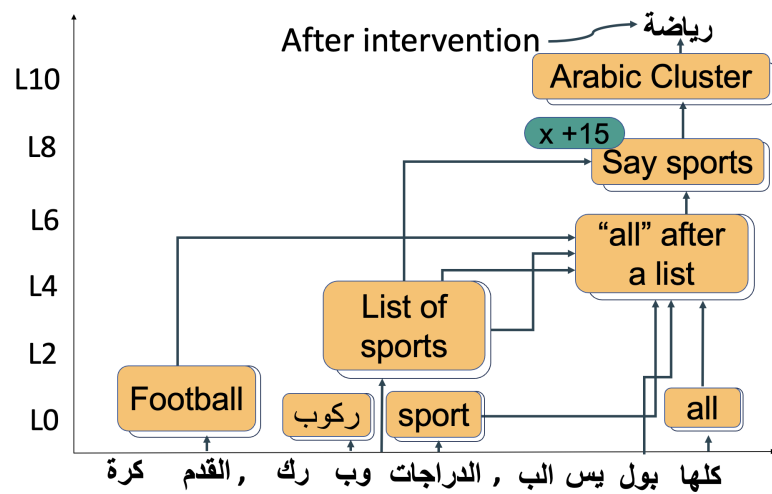


Figure 36. Scaling up the "Say Sports" cluster makes the model predict the right answer.

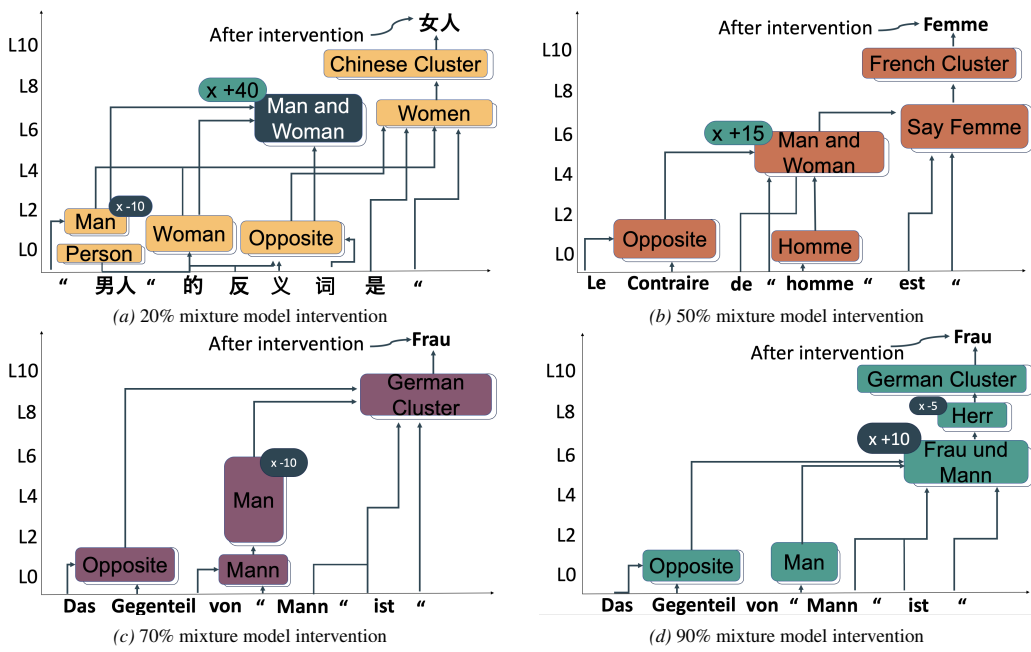


Figure 37. Intervention examples where appropriate scaling switches the model’s answer to the correct response.

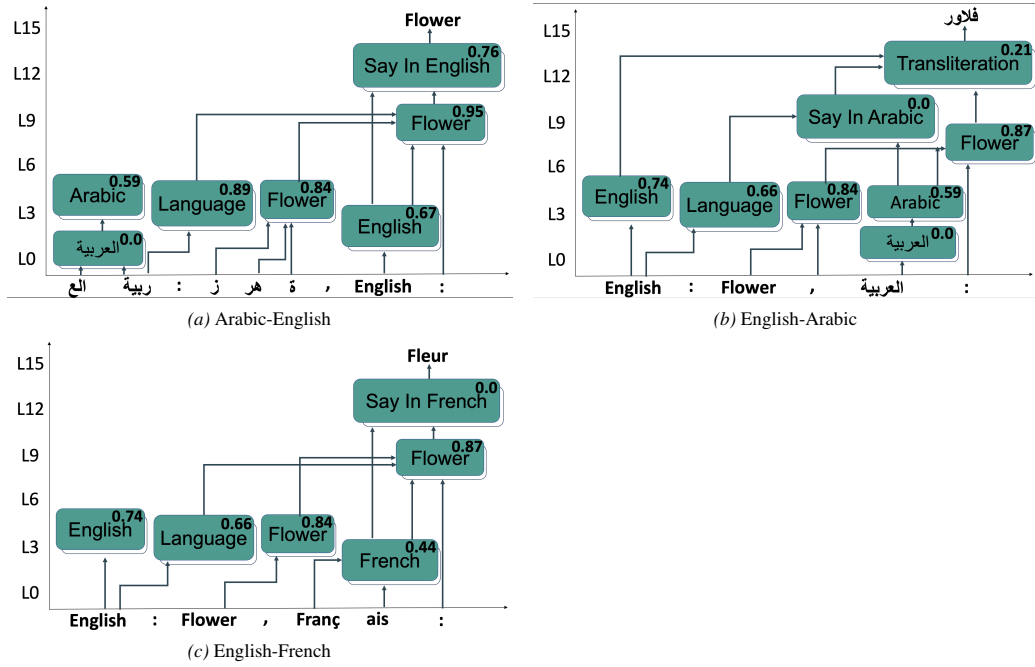


Figure 38. Circuits for the translation task.

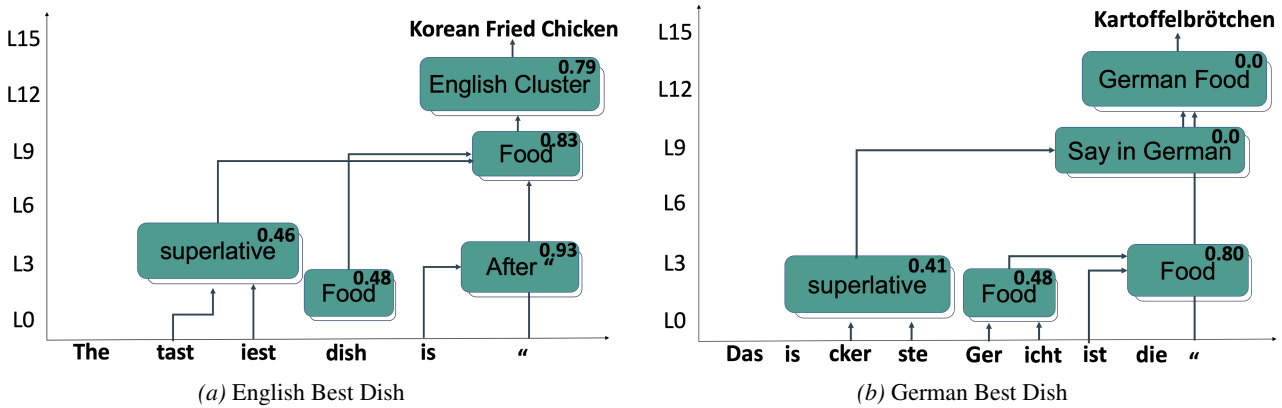


Figure 39. Circuits for the cultural task.

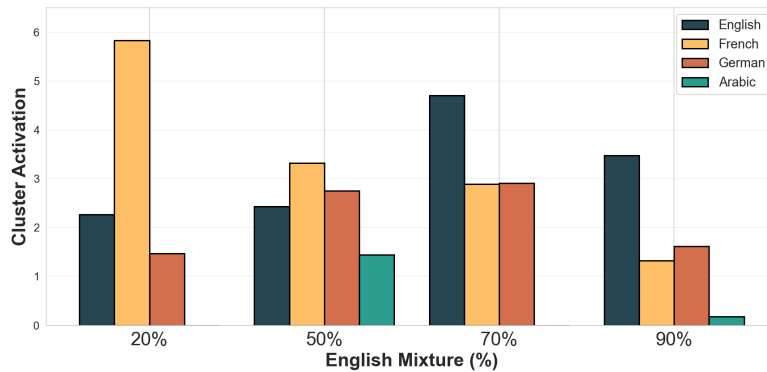
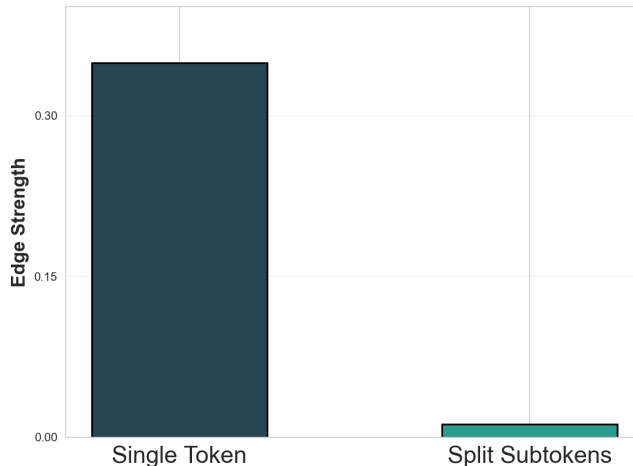


Figure 40. Cluster activation strength across languages and mixture ratios. English shows consistently higher activations for task-relevant clusters (Man&Woman for Antonym, Say Sports for Category Completion), with disparities diminishing at the 20% mixture.


 Figure 41. Edge strength from token embeddings to target clusters versus sub-tokenization rate. Higher sub-tokenization correlates with weaker edge strength ($r=-0.82$), explaining reduced circuit activation in fragmented languages like Arabic.

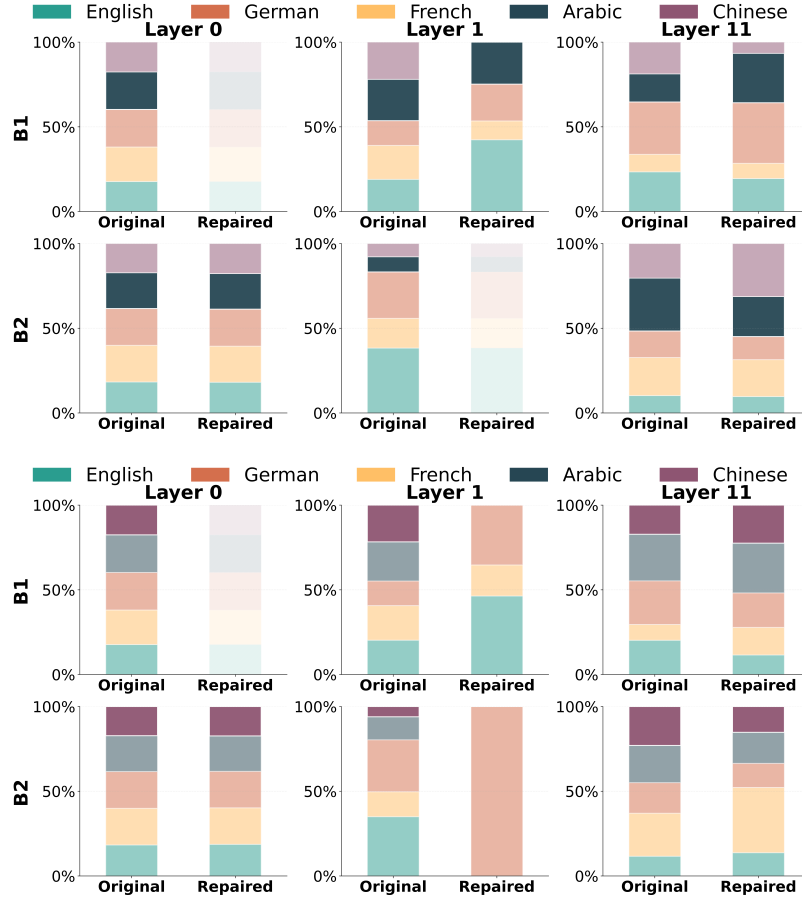


Figure 42. Language distribution comparison across layers and buckets for Arabic (top) and Chinese (bottom).

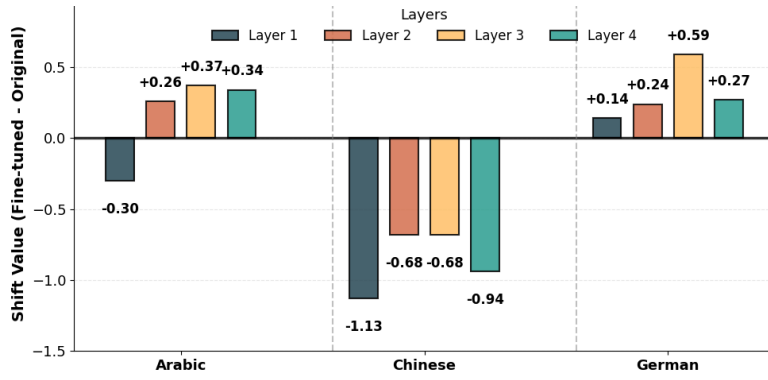


Figure 43. Logit Lens token assembly results. We find that models tend to repair early layers by making them better at assembling tokens, thus generalizing to abstractions earlier. This especially applies to Arabic and German. Surprisingly, Chinese finetuning results in less assembly across layers. This is in accordance with the higher-rank update of Chinese that shows that the model is possibly pattern-matching.